Electrical Conductivity of Rocks and Dominant Charge Carriers
Part I: Thermally Activated Positive Holes

Friedemann Freund and Minoru M. Freund*

NASA Ames Research Center
MS 245-4
Moffett Field, CA 94035-1000
Tel. +001 650-604-5183
Fax +001 650-604-4680
e-mail friedemann.t.freund@nasa.gov
++++++++++++++++++++++++++++++
Department of Physics
San Jose State University
++++++++++++++++++++++++++++++
Senior Scientist
Carl Sagan Center, SETI Institute
++++++++++++++++++++++++++++++

* NASA Ames Research Center
Center for Nanotechnology and Advanced Space Materials
Moffett Field, CA 94035-1000

Abstract

The prevailing view in the gophysics community is that the electrical conductivity structure of the Earth's continental crust over the 5-35 km depth range can best be understood by assuming the presence of intergranular fluids and/or of intergranular carbon films. Based on single crystal studies of melt-grown MgO, magma-derived sanidine and anorthosite feldspars and upper mantle olivine we present evidence for the presence of electronic charge carriers, which derive from peroxy defects that are introduced during cooling, under non-equilibrium conditions, through a redox conversion of pairs of solute hydroxyl arising from dissolution of H_2O. The peroxy defects become thermally activated in a 2-step process, leading to the release of defect electrons in the oxygen anion sublattice. Known as positive holes and symbolized by $h^{\bullet}$, these electronic charge carriers are highly mobile. Chemically equivalent to O^{-} in a matrix of O^{2-} they are highly oxidizing. Being metastable they can exist in the matrix of minerals, which crystallized in highly reduced environments. The $h^{\bullet}$ are highly mobile. They appear to control the electrical conductivity of crustal rocks in much of the 5-35 km depth range.

Keywords

Electrical conductivity, igneous rocks, non-equilibrium conditions, peroxy defects, positive holes, metastable electronic charge carriers, dc conductivity, dielectric polarization.

42

* deceased

I Introduction

For many geophysical processes in the Earth's crust it is crucially important to understand the nature of the charge carriers, which control the electrical properties of rocks. In this report we focus on conditions in the Earth's continental crust over the 5-35 km depth range, where most major crustal earthquakes occur. Our goal is to identify the electric charge carriers that are present or can be activated in this depth range.

Any cursory inspection of geological maps reveals how heterogeneous the crust can be. Magneto-telluric (MT) soundings have provided ample evidence for the electrical heterogeneity as a function of depth. However, they have also identified high conductivity zones that seem to consistently exist at certain crustal depth levels, as well as large-scale inhomogeneities in the upper mantle.

The two most widely quoted causes for variations in the electrical properties of rocks are interconnected networks of aqueous fluids and/or of intergranular carbon or graphite films [Glover 1996]. In this report we point to the presence of electronic charge carriers in minerals and rocks, which have not been fully recognized in the past.

Any electrical charge transport in rocks can be attributed to one or more of the following three contributing causes: (i) electrolytic conduction, (ii) electronic conduction, or (iii) ionic conduction. Electrolytic conduction will occur in rocks where aqueous fluids fill pores and the intergranular space, forming an interconnected network. Ionic transport is negligible at the temperatures most relevant for the crustal depth range of interest here but surely becomes important at high temperatures, both in the solid state and with the on-set of partial melting. Electronic conduction can occur over the entire temperature range of interest here, either through intergranular networks or through the bulk.

I.1 Emphasis on Intergranular Fluids and on Carbonaceous Films

Aqueous fluids certainly exist in the shallow crust in the form of saline solutions filling the omni-present pore space in rocks. Open pores can form a communicating network through which fluids are able to flow under the influence of tectonic pressure gradients. Such forced fluid flow through narrow pores will produce electrical signals, known as streaming potentials. They arise when cations are preferentially retained along the walls of narrow conduits while anions are swept along with the fluids [*Dobrovolsky et al.*, 1989]. Streaming potentials are the foundation of the electrokinetic effect, widely used in prospecting of the shallow crust by magneto-telluric and other techniques as well in attempts to understand pre-earthquake electrical or electromagnetic signals [*Merzer and Klemperer*, 1997; *Mitzutani et al.*, 1976; *Takahashi et al.*, 2007; *Teisseyre*, 1983; *Yoshida et al.*, 1998].

Deeper into the crust, as the overload of the rock column increases, pores that communicate with the surface must close as the difference between lithostatic and hydrostatic pressures becomes too large. Closing occurs around 3-5 km. Below this cap, fluids are at lithostatic pressures. They can either be trapped *in situ* in sediment-derived formations, which had been transported downward through tectonic processes such as faulting [*Yardley et al.*, 2000], or be supplied from below through degassing of magmas during crystallization or through mineral dehydration above a mantle plume [*Vanyan and Gliko*, 1999] or above a subducting slab [*Hyndman*, 1988]. The presence of an electrolytically conductive intergranular phase should have a profound effect on the electrical conductivity structure.

Two views emerged in the literature regarding the nature of intergranular films. One view emphasizes the presence of "water". The other view emphasizes the presence of carbon films precipitated in the

intergranular space out of CO/CO_2–bearing fluids within the stability field of graphite [*Constable and Duba*, 1990; *Nover et al.*, 2005; *Shankland et al.*, 1997].

The inferred presence of water has been widely invoked as an explanation for increased electrical conductivities in the crust and the upper mantle [*Frost and Bucher*, 1994; *Fuji-ta et al.*, 2004; *Iio et al.*, 2002; *Karato*, 2011; *Khan and Shankland*, 2011b; *Nekut et al.*, 1977; *Qin et al.*, 1992; *Wannamaker*, 1994] or to explain high conductivity layers in the crust at a certain depth ranges, around 20 km [*Chen and Chen*, 2002; *Fuji-ta et al.*, 2004; *Lee et al.*, 1983; *Patro et al.*, 2005; *Qin et al.*, 1992]. The zones of high electrical conductivity seem to correlate with zones of low velocity for seismic waves, though this correlation has been called into question [*Bai et al.*, 2002]. The presence of water has also been invoked to account for high electrical conductivity along seismically active faults such as the Parkfield section of the San Andreas Fault in California [*Unsworth et al.*, 1999].

Intergranular carbon, carbonaceous or graphite films have been considered as an alternative to water [*Nover et al.*, 2005; *Olhoeft*, 1981; *Shankland et al.*, 1997]. Carbon films have been invoked in the context of zones of high crustal conductivity around 20 km, the presence of which suggests conduction mechanisms that are not activated in at shallower depth and disappear at greater depth [*Glover*, 1996; *Haak and Hutton*, 1986; *Hyndman et al.*, 1993].

Surface analytical techniques such as x-ray photoelectron spectroscopy (XPS), secondary ion mass spectrometry (SIMS) or ion probes have indeed provided evidence for carbonaceous surface films a few atomic layers thick after rocks had been fractured in 95% CO_2 +5% CO or 5% CH_4 gas mixtures at temperatures between 350–500°C [*Roberts et al.*, 1999]. Such films are assumed to have been deposited *in situ* from fluids containing reduced carbon species such as CO or CH_4 that would have percolated through the rocks. Experiments with thin carbon films along the contact between two quartz crystals at 1 GPa have demonstrated that, when the temperature was raised to about 630°C, the graphite films disintegrate and disappear [*Yoshino and Noritake*, 2011].

In the petrological literature a strong case has been made that the stable lower crust should be "dry" and devoid of percolating or stagnant fluid phases [*Yardley and Valley*, 1997]. The argument is that, given the prevailing high temperatures, any "water" in these deep environments will be consumed rapidly – on a geological time scale – by metamorphic reactions leading to hydroxyl-bearing minerals such as amphiboles and mica, both of which are characterized by low electrical conductivities [*Litovchenko and Mazykin*, 1984; *Meunier et al.*, 1983; *Wang et al.*, 2012]. The case for a "dry" lower crust has sparked an insightful discussion about alternative views [*Wannamaker*, 1999; *Yardley and Valley*, 2000].

I.2 AC versus DC

Numerous laboratory studies have been conducted to characterize the electrical properties of minerals and rocks. Most often the electrical conductivity was measured using ac methods. The reason for preferring is that ac measurements can (i) provide more parameters than dc techniques and (ii) are better suited for experiments under the high temperatures and high pressures needed to explore the electrical properties of minerals and rocks under lower crust and upper mantle conditions [*Fuji-ta et al.*, 2004; *Liu et al.*, 1999; *Nover*, 2005; *Wang et al.*, 2012; *Yang*, 2011].

When an ac electric field is applied, a marked frequency dependence is often observed, which is caused by the complex interplay between conduction and displacement currents. Displacement currents from the polarization of electrons, bonds, mobile ions, defects that either have a dipole or develop a dipole in the alternating electric field, charges accumulated along grain boundaries or

charges trapped and detrapped at the interfaces between the sample and the electrodes.

To appreciate the complexity of the situation we look at the resistivity ρ [Ω cm] or its reciprocal, the conductivity σ [$\Omega^{-1}cm^{-1}$], and at the dielectric permittivity ε [F cm^{-1}]. For a linear system we can write the conduction current density J_{totsl} at time t and the electric displacement D caused by an electric field E:

$$J_{total} = \sigma E + \varepsilon \delta E/\delta t \quad [1]$$

and

$$D = \varepsilon E \quad [2]$$

The relative dielectric constant ε_r of the medium is defined as

$$\varepsilon_r = \varepsilon/\varepsilon_0 \quad [3]$$

where $\varepsilon_0 = 8.854 \times 10^{-12}$ [F/m] is the dielectric permittivity of free space. Conduction currents and displacement currents will be out of phase with each other.

The parameters that are actually measured are not the true values but the effective values given by

$$\varepsilon_{eff}(\omega) = \varepsilon'(\omega)\ \omega\varepsilon'' \quad [4]$$

and

$$\varepsilon_{eff}(\omega) = \varepsilon'(\omega) - i(\omega)\sigma''(\omega)/\omega \quad [5]$$

The ratio of the imaginary part to its real part defines the phase angle Ψ given as:

$$\tan\delta = [\omega\varepsilon''(\omega)]/\sigma'(\omega) \quad [6]$$

(a)

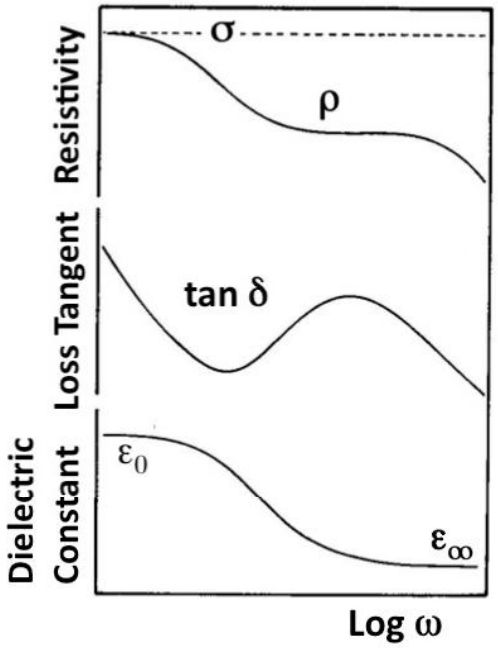

***Figure 1a**: Resistivity ρ, loss tangent, tan δ, and dielectric constant ε as a function of frequency ω. The "true" conductivity σ defined for $\omega = 0$.*

(b)

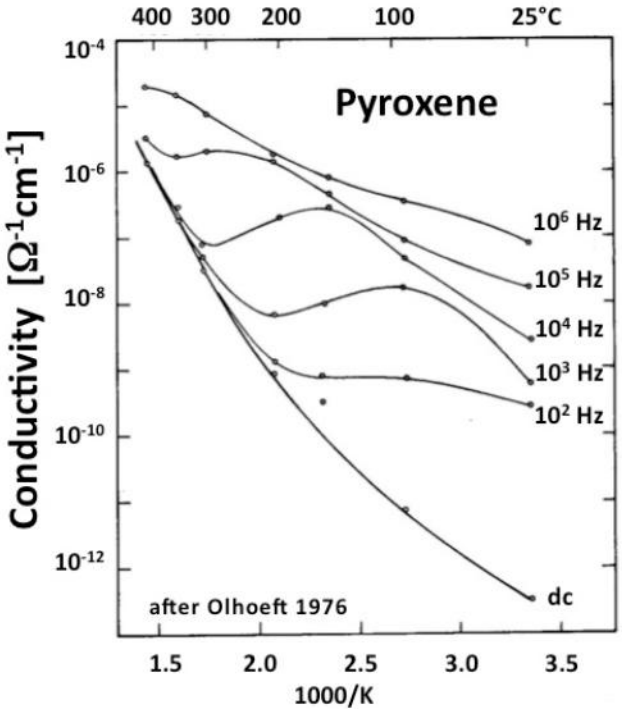

***Figure 1b**: Example of the conductivity σ of a pyroxene as a function of temperature from 25 to 400°C and 0 to 10^6 Hz [Olhoeft, 1976].*

Figure 1a illustrates how the resistivity ρ, the loss angle tan δ, and the effective dielectric constant ε_{eff} depend upon the frequency ω. The "true" conductivity σ is defined only at 0 Hz. **Figure 1b** shows the

conductivity σ of a pyroxene between 25°C to 400°C at frequencies ω between 0 Hz and 10^6 Hz [*Olhoeft*, 1976]. A frequency-dependent loss feature is seen, which shifts to higher temperatures with increasing frequencies but also becomes increasingly indistinct.

Data as depicted in **Figure 1b** have diagnostic value for the interpretation of laboratory experiments. However, they are not directly useful in the analysis of many sets of field data collected by MT techniques. The reason is that, while the first few hundred meters below the surface with EM waves in the 1-5 kHz range, low to ultralow frequencies in the Hz, mHz and μHz ranges are needed to penetrate deep enough into the Earth to send back information about the electrical structure of the deeper regions of the Earth [*Cagniard*, 1953].

In order to build the case for dc measurements, it is opportune to take a step back and look at the electronic conductivity of materials from a broader perspective.

Electronic Charge Carriers

Materials can be broadly classified into three groups: metals, semiconductors, and insulators. The three groups differ in the position of their valence bands (VB) and conduction bands (CB) relative to each other on the energy scale.

In metals, VB overlaps with CB allowing electrons from the VB to flow over into the CB. The CB electrons are not bound to any particular atom, meaning that their wavefunctions are delocalized.

Semiconductors have a modestly wide band gap, E_g on the order of 1 eV. Such gaps allow some electrons from the VB to become thermally activated to the CB, where they act as negative charge carriers e'. Around 300 K the thermal energy kT is ~25 meV, where k is the Boltzmann constant, 8.618×10^{-5} eV/deg, and T the absolute temperature. Assuming a Boltzmann distribution, the probability for VB electrons to be thermally activated across E_g is $e^{-Eg/kT}$. For a 1 eV band gap this means $e^{-40} \sim 4 \times 10^{-18}$ at 300 K. Electrons that make the transition to the CB leave behind defect electrons in the VB. The defect electrons are called holes, designated by $h^{\bullet}$. They carry a +1 charge. Holes in the VB are less mobile than electrons on the CB.

In insulators, E_g is wide to very wide, often 5 eV or more. Thus the probability for electrons to be thermally activated from VB to CB becomes vanishingly small. Numerically, for $e^{-Eg/kT} \sim 5$ eV, the probability at 300 K or room temperature is on the order of 10^{-87} and still as low as 10^{-29} for 900 K or ~630°C. Thus, the electronic conductivity of insulators should be zero. Any observed conductivity has to arise from the presence of defects and/or impurities.

Eq. [7] links conductivity to the number density of charge-carrying species n and their mobility μ:

$$\sigma = n \mu z^2 e^2/(kT) \qquad [7]$$

where z is the valence of the conducting species, e the unit charge, k the Boltzmann constant, and T the absolute temperature.

If the conductivity is thermally activated with an activation energy E_{act}, we have:

$$\sigma = \sigma_0 \exp [-E_{act}/kT] \qquad [8]$$

where the pre-exponential factor σ_0 is the product of several contributions including μ, z and e. If more than one process control the conductivity, each with an activation energy E_1, E_2 …, we have:

$$\sigma = \sigma_1 \exp [-E_1/kT] + \sigma_2 \exp [-E_2/kT] + \ldots \qquad [9]$$

Plotting log σ versus 1/T eq. [8] will give a straight line, called an Arrhenius plot, with the slope E_{act}. Eq. [9] will give two or more straight sections corresponding to E_1, E_2…

In semiconductors electrons in the CB, e', always compete with holes in the VB, $h^{\bullet}$. The overall

conductivity behavior depends on at the number densities of e' and $h^{\bullet}$, designated as n' and $n^{\bullet}$, and the mobilities, designated as μ' and $\mu^{\bullet}$. If the product $n'\mu'$ is larger than $n^{\bullet}\mu^{\bullet}$, electrons control the overall conductivity and the semiconductor is said to be n-type. Conversely, if the product $n'\mu'$ is smaller than $n^{\bullet}\mu^{\bullet}$, holes control the conductivity and the semiconductor is said to be p-type.

$$n'\mu' > n^{\bullet}\mu^{\bullet} \quad \text{n-type} \qquad [10a]$$

$$n'\mu' < n^{\bullet}\mu^{\bullet} \quad \text{p-type} \qquad [10b]$$

Any semiconductor that is chemically pure is said to be intrinsic. In the intrinsic case, when electrons are thermally promoted across E_g, the number of electrons on the CB will be equal to the number of holes in the VB: $n' = n^{\bullet}$. Since the mobility of electrons on the CB is always higher than the mobility of holes in the VB, any intrinsic semiconductor will be n-type. While n' and $n^{\bullet}$ depend exponentially on the temperature, the temperature dependence of the mobilities, μ' and $\mu^{\bullet}$ is weak.

If a semiconductor is doped with aliovalent impurities, it can be made more n-type or p-type depending on the nature and concentrations of the dopants. Aliovalent dopants mean impurities with valencies other than those of the regular lattice constituents of the semiconductor material. However, aliovalency can also involve native lattice constituents of the semiconductor in a different valence state. This aspect will play an important role in the discussion below.

The electrical conductivity of a material is the sum of the conduction of each type of charge carriers or each type of defects, all acting in parallel:

$$\sigma = \Sigma\sigma_i = \Sigma\, n_i\, z_i\, \mu_i \qquad [11]$$

where n_i is the concentration of the i^{h} type of charge carrier, z_i is the charge, and μ_i the mobility.

Minerals and rocks are "dirty" systems with complex chemistries and defects of many different kinds always present over a range of number densities or concentrations. Each type of impurity or defect contributes to σ, though usually not more than two types will dominate in any given temperature window under a given set of thermodynamic conditions.

Activation Energies, Charge Carrier Concentrations and Mobilities

Figures 2a/b show Arrhenius plots for mafic and ultramafic igneous rocks samples that have been conditioned by cycling them through the temperature interval of interest under controlled redox conditions, using a variety of heating and cooling rates [*Parkhomenko*, 1967; *Parkhomenko*, 1982].

From below 100°C to about 600-700°C, σ for all rocks under study is consistent with eq. [8], i.e. with a single conductivity mechanism characterized by a single value of E_{act}. Remarkably E_{atc} is closely the same for all rocks, ~1 eV. This suggests that, irrespective of the type of rock and in spite of mineralogical and chemical differences, the conductivity of these rocks appears to be controlled by the same conductivity mechanism over the low temperature region (LT), from below 100°C to 600-700°C.

Different samples of the same rock produce straight sections of the Arrhenius plots that can be shifted parallel to each other on the log σ scale by a significant amount. Hence, in the ΔT window shown here, the only difference is the numerical value of σ_0. According to eq. [7] the only T-dependent contributions to σ_0 are n and μ, the number density of charge carriers and their mobilities, respectively. Since the temperature dependence of the mobility is weak, we can treat μ' and $\mu^{\bullet}$ as approximately constant across the temperature interval of interest here, Hence our focus can center on n' and $n^{\bullet}$.

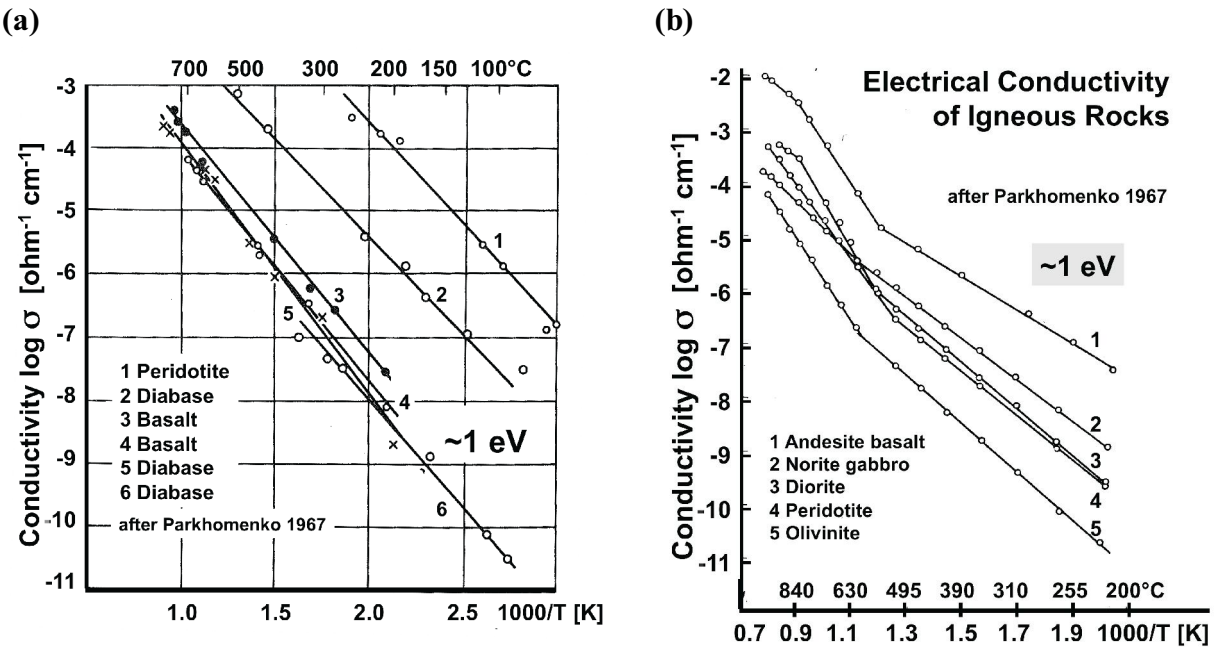

Figure 2a/b: Electrical conductivity of mafic and ultramafic rocks after [Parkhomenko, 1982].

Figure 2b shows that, when the rock samples were heated beyond 550-600°C, up to about 1000°C, straight sections with different slopes are obtained, suggesting different E_{act} values for the high temperature (HT) region.

The two linear sections points to two conduction mechanisms, endowed with activation energies, E_1 in the LT range and E_2, E_3, E_4 … in the HT range, as suggested by eq. [9]. At HT ionic conductivity sets in, exhibiting different slopes for different rock types, suggesting different ionic conduction with different E_{atc} values. At the same time E_{atc} in the LT range is closely the same for all rocks, although the σ_0 values may vary over orders of magnitude, even for the same rock type. For instance, the Arrhenius plot for peridotite in **Figure 2a** shows a conductivity over the 50-300°C window that is 6 orders of magnitude higher than the conductivity of the peridotite shown in **Figure 2b** over the 100-500°C window.

The constancy of the activation energy $E_{act} \sim 1$ eV across different rock types in the LT range is as remarkable as the widely different σ_0 values within one rock type.

Nature of the Charge Carriers

MgO, a II-VI material, is not a semiconductor. It has a very wide band gap of about 8 eV, MgO is the most ionic among all alkaline earth oxides with mostly Coulombic interaction between Mg^{2+} and O^{2-} [*Pacchioni et al.*, 1993]. As a main-group element with the electronic configuration $1s^2\ 2s^2$, Mg has only one stable oxidation state, 2+. Therefore, pure MgO should be a model insulator.

Large MgO single crystals can be melt-grown by the carbon arc fusion technique [*Abraham et al.*, 1971]. Crystals are available at nominal 99.9% purity grades, designated as 3N, either undoped or doped with various levels with divalent 3d transition elements Mn, Fe, Co, or Ni. Purer MgO crystals, up to purity grade 99.99%, designated as 4N, are also available in sizes up to several cm^3.

If MgO single crystals are well-annealed, their electrical conductivity at room temperature can be

below 10^{-16} [$\Omega^{-1}cm^{-1}$]. However, when heated, MgO single crystals display a striking dc conductivity behavior as illustrated in **Figures 3a-d** for a high purity 4N-MgO crystal measured under the most stringent clean conditions and with a guard electrode to remove contributions from surface conductivity [*Kathrein and Freund*, 1983].

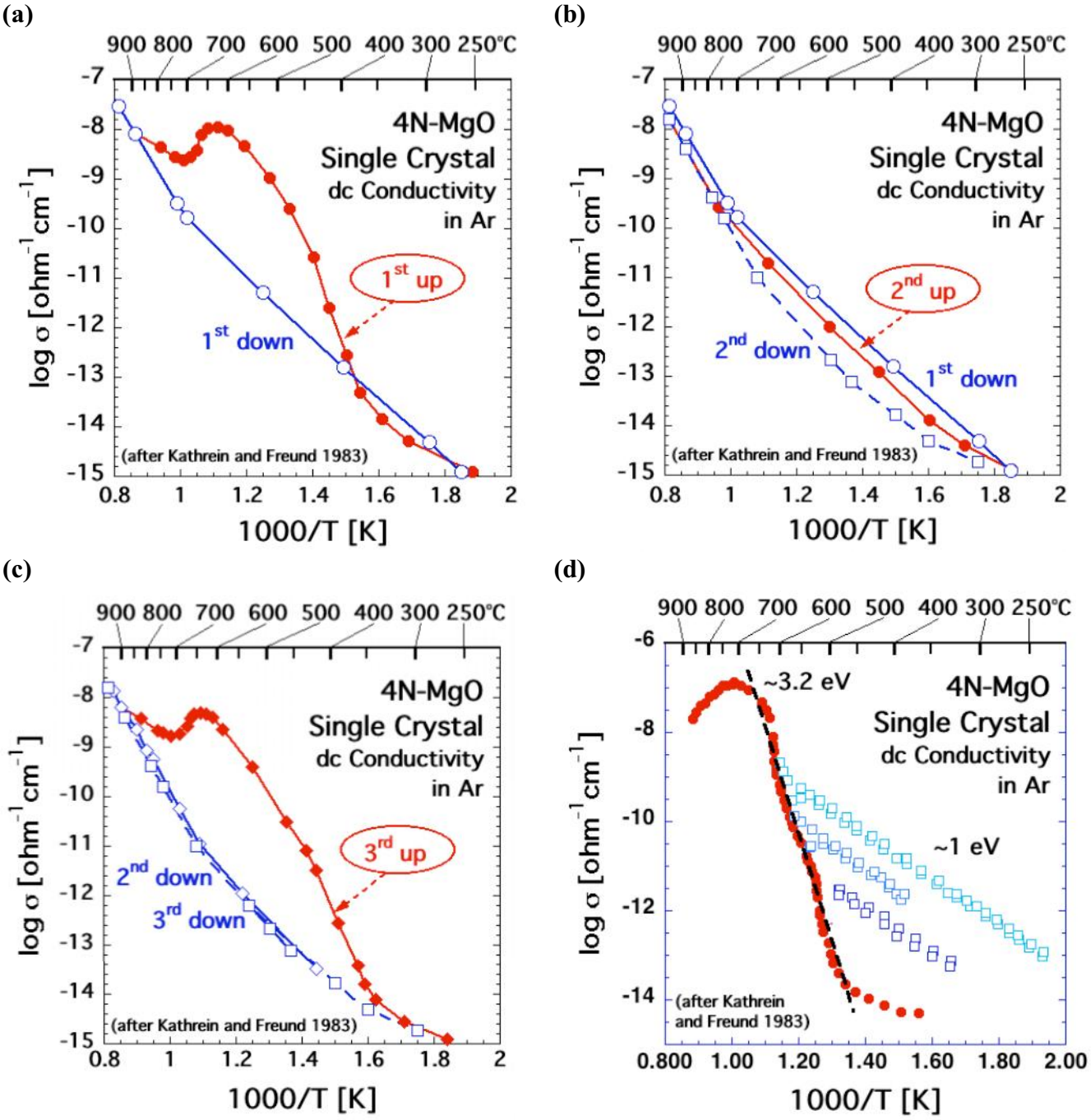

Figure 3. *Sequence of dc conductivity measurements of a highest purity grade MgO single crystal under the most stringent clean conditions.* ***(a)*** *shows an anomalous increase in conductivity during the first heating, which is not observed as shown in* ***(b)*** *when the crystal is reheated immediately after cooling. However, if the crystal is annealed for several hours, the anomalous conductivity reappears as shown in* ***(c)***. *Panel* ***(d)*** *shows that this anomalously high conductivity is due to the activation of charge carriers that conduct electricity with an activation energy ~1 eV [Kathrein and Freund, 1983].*

Upon first heating, starting around 350-400°C, the conductivity of the MgO crystal increases by about 6 orders of magnitude as shown in **Figure 3a.** At the heating rate used in this experiment, 10° min^{-1}, the conductivity reaches a maximum around 600-650°C and then decreases, only to increase again above 700°C. Around 850-900°C the conductivity joins an Arrhenius straight section that describes the reversible HT conductivity, which is endowed with an activation energy of 2.4 eV. At very slow cooling rates the HT mechanism can be followed downward to below 500°C [*Lempicki*, 1953]. At any cooling rate the HT mechanism is eventually replaced by an LT mechanism, endowed with an activation energy of ~1 eV. The transition from HT to LT occurs around 650-700°C. In the HT regime the electrical conductivity of MgO is controlled by Mg^{2+} diffusion via an Mg^{2+} vacancy hopping mechanism [*Sempolinski and Kingery*, 1980], possibly augmented by O^{2-} diffusion [*Wuensch et al.*, 1973]. The nature of the LT 1 eV mechanism has long remained undetermined.

If the MgO crystal is reheated immediately after cooling as in the run depicted in **Figure 3b**, the conductivity curve "2nd up" closely follows the LT conductivity behavior observed during first cooling "1st down" and also during second cooling "2nd down". If, however, the MgO crystal is not reheated immediately after cooling but allowed to anneal for several hours or overnight at temperatures below ~150°C, **Figure 3c** shows a conductivity pattern, "3rd up", similar to that of the first heating, "1st up" in **Figure 3a**. This conductivity pattern is reproducible except that, during repetitive heating-cooling cycles, the highest conductivity achieved around 650°C slowly decreases with the number of cycles and with the holding time at the highest temperature. Another subtle but reproducible feature is that, during cooling, the transition from the HT section to LT section shifts to ever lower temperatures the more often the MgO crystal has been cycled through HT and the longer it has been kept at temperatures >900°C.

A similar conductivity pattern has been observed in studies with natural samples, both single crystal minerals and rocks [*Constable and Duba*, 1990; *Duba and Constable*, 1993; *Roberts et al.*, 1999]. In those cases the high conductivity recorded during first heating in the LT range has been blamed on adventitious surface contamination by carbonaceous films. Surface contamination can never be totally ruled out during conductivity measurements, even under very well controlled conditions. However, conductivity measurements can be performed in such a way that surface contamination as a reason for the anomalous electrical conductivity behavior can be ruled out [*Kathrein and Freund*, 1983].

Figure 3d shows what happens when the heating of the 4-N MgO crystal is intermittently reversed three times within the range of the anomalously rapid conductivity increase, at 540°C, 555°C, and 590°C. After each intermediate cooling, the MgO crystal was immediately reheated. For every cycle, Arrhenius straight sections are obtained, all with the same slope corresponding to an activation energy of ~1 eV. Each time, during reheating, the conductivity eventually rejoins the main branch, marked by solid red circles. The main branch is characterized by an E_{act} value around 3.2 eV.

Because this particular experiment was conducted at heating and cooling rates of 20°C min^{-1}, the main branch in **Figure 3d** is shifted towards higher temperatures relative to the curves in **Figures 3a-c**, which were conducted at 10° min^{-1}. Except for this experimental effect, which due to the thermal inertia of the system, the conductivity patterns are very similar.

A conductivity pattern as depicted in **Figure 3d** is not consistent with surface contamination. It points to two processes working in tandem.

Process (i) involves the activation of defects in the MgO structure, which are electrically inactive but release mobile charge carriers as the temperature increases. These charge carriers must be electronic. The activation begins at a threshold temperature, ~350°C at the 10° min^{-1} heating rate or ~450°C at the 20° min^{-1} heating rate, and has an apparent activation energy barrier ($E_1 + E_2$) ~3.2 eV. Process (i) is

consistent with the number n of mobile charge carriers increasing exponentially as the MgO crystal is heated. Process (i) takes place only after the MgO crystal has been annealed for some time, operating between 350-600°C during the 10° min^{-1} runs or 450-650°C during the 20° min^{-1} run. Around 600-650°C process (i) comes to an end, suggesting that all available charge carriers have been activated. Above 700°C the conductivity decreases, indicating that charge carriers are being destroyed. This is consistent with the aforementioned decrease in maximum conductivity value obtained during consecutive heating-cooling cycles.

Once the charge carriers are activated, they remain active for a sufficiently long time to immediately conduct successive cooling-reheating cycles. If the MgO crystal is allowed to anneal, the charge carriers return to an inactive state, from which they can be reactivated by reheating to 350-450°C.

Process (ii) relates to how much current is carried by n mobile charge carriers, where n is the number of charge carriers activated through process (i). The charge carriers require an activation energy E_2 to jump from one site to the next. Both processes, (i) with the combined activation energy $(E_1 + E_2) \sim$ 3.2 eV, and (ii) with the activation energy $E_2 \sim 1$ eV, follow Arrhenius relations. To describe the system under study we can use a relation very similar to eq. [9]:

$$\sigma = \sigma_0 \exp [-(E_1+E_2)/kT] \qquad [12]$$

The sum $(E_1 + E_2)$, ~3.2 eV, applies to the main heating branch in **Figure 3d**. $E_2 \sim 1$ eV applies to the cooling-reheating straight sections in **Figures 3a-d**. The value for E_1 is ~2.2 eV, that for E_2 is ~1 eV.

In summarizing this section we can state with confidence that highest purity-grade 4N-MgO single crystals exhibit a complex dc conductivity behavior in the temperature window between ambient and 800-900°C. The conductivity increase by at least 6 orders of magnitude between 300°C and 600-700°C is clearly at odds with the presumed model insulator nature of MgO. It points to either the presence of impurities that are not included in the chemical purity grade or to the presence of defects, which had not been identified in prior work.

There is one more important observation: MgO crystals doped with divalent 3d transition metal cations, Mn^{2+}, Fe^{2+}, Co^{2+} or Ne^{2+} at various, even high concentration levels exhibit the same electrical conductivity pattern as described here for 4N-grade MgO [*Freund et al.*, 1993; *Kathrein and Freund*, 1983]. This suggests that the anomalous conductivity behavior is not caused by transition metal impurities nor by charge carriers that would propagate via the metal cation sublattice.

Furthermore we can state with confidence that the observed conductivity behavior of the MgO single crystals and their 1 eV conductivity mechanism cannot be due to surface contamination. MgO crystals that were temperature-cycled in pure O_2 show the same conductivity pattern, ruling out that the increased conductivity would be caused by carbonaceous surface films [*Kathrein and Freund*, 1983].

Valence Changes in the Oxygen Anion Sublattice

MgO was the first oxide material for which evidence was obtained that the valence of oxygen anions is not fixed at 2-, as is widely assumed, but can change to the higher oxidation state 1-. When ultrahigh purity $Mg(OH)_2$ was thermally decomposed to MgO + H_2O, forming a dilute MgO–H_2O solid solution, $Mg_{1-\delta}(OH)_{2\delta}O_{1-2\delta}$, it released copious amounts of H_2, 10,000 ppm, even though the transition metal impurity level was <5 ppm, equivalent to a purity grade >99.999% [*Martens et al.*, 1976b]. Since Mg cations are fixed in their 2+ valence state, the only possibility for H^+ to be reduced to H_2 was to concomitantly oxidize oxygen anions from valence 2- to valence 1-.

Follow-on studies with MgO single crystals revealed that the redox conversion takes place in the MgO

matrix involving OH^- pairs associated with and chargewise compensated by Mg^{2+} vacancies. During the redox conversion two hydroxyl protons are reduced to H, forming H_2, while two hydroxyl oxygen are oxidized to O^-, forming a peroxy anion, O_2^{2-} [*Batllo et al.*, 1991; *Freund and Wengeler*, 1982].

Using the Kröger-Vinck point defect designation[1] we can write this reaction as:

$$[OH^{\bullet}\ V_{Mg}^{''}\ HO^{\bullet}]^x \Leftrightarrow [O_O^{\bullet\bullet}\ (H_2)_{Mg}^{''}]^x \qquad [13]$$

The defect on the right hand side can release its H_2 molecule into an interstitial site:

$$[O_O^{\bullet\bullet}\ (H_2)_{Mg}^{''}]^x \Leftrightarrow [O_O^{\bullet\bullet}\ V_{Mg}^{''}]^x + (H_2)_i^x \qquad [14]$$

where the right side now describes an Mg^{2+} vacancy chargewise compensated by a peroxy anion, O_2^{2-}. If the MgO crystals are small [*Martens et al.*, 1976a] or if the time for outdiffusion is long, the H_2 can escape from the solid matrix. Such loss of H_2 would change $Mg_{1-\delta}(OH)_{2\delta}O_{1-2\delta}$ into $Mg_{1-\delta}O$. If $\delta \ll 1$, cation-deficient $Mg_{1-\delta}O$ may also be written as $MgO_{1+\delta}$.

MgO is intrinsically diamagnetic. Peroxy anions are diamagnetic, because the two O^- are tightly coupled and spin-paired. Upon heating, the spin pairing loosens up and eventually breaks, causing a transition from a diamagnetic to a paramagnetic state and dissociation. Magnetic susceptibility studies have provided information about this transition [*Batllo et al.*, 1991]. Peroxy spin decoupling and dissociation take place in two distinct steps: (i) the peroxy bond loosens up, (ii) full dissociation takes place. Designating as I the peroxy defect as **I** and as **II** the transition state, where spins associated with the two O^- begin to decouple, we have:

$$[O_O^{\bullet\bullet}\ V_{Mg}^{''}]^x \Leftrightarrow [O^{\bullet}\ V_{Mg}^{''}\ O^{\bullet}]^x \qquad [15]$$
$$\mathbf{I} \Leftrightarrow \mathbf{II}$$

During stage **II**, the wave functions associated with the two O^- delocalize over many neighboring oxygen anion positions, causing anomalies in fundamental physical properties such as in the thermal expansion and in the refractive index [*Freund et al.*, 1994]. However, at this decoupling stage, there is no significant increase in the electrical conductivity.

During stage **II**, the two O^- dissociate. Dissociation involves an electron transfer from a neighboring O^{2-} donates into the $[O^{\bullet}\ V_{Mg}^{''}\ O^{\bullet}]^x$ defect. The neighboring O^{2-}, which had donated the electron, thereby turns into an O^-, which is no longer bound to the Mg^{2+} vacancy. It becomes an unbound defect electron on the oxygen anion sublattice. The Mg^{2+} vacancy retains one O^-, forming a V^- center, a point defect widely studied by electron paramagnetic resonance spectroscopy [*Henderson and Wertz*, 1977; *Marfunin*, 1979]. Designating the dissociated state with **III** we have:

$$[O^{\bullet}\ V_{Mg}^{''}\ O^{\bullet}]^x \Leftrightarrow [O^{\bullet}\ V_{Mg}^{''}]' + O^{\bullet} \qquad [16]$$
$$\mathbf{II} \Leftrightarrow \mathbf{III}$$

Figure 4 outlines the temperature windows for the transitions between defects **I**, **II**, and **III**. It summarizes the insight gained from a wide range of studies aimed at understanding the electrical conductivity of nominally high purity MgO single crystals. These studies have positively identified peroxy defects in the MgO matrix as the cause for this anomalous conductivity behavior.

[1] V stands for vacancy; subscripts identify the site (except for oxygen sites, where subscripts are omitted); superscript prime, dot, and x designate single negative, positive and neutral charges, respectively, double prime and double dot designate double negative and positive charges; subscript i means interstitial; square brackets outline the essential parts of any given point defect.

Unbound O^- constitute defect electrons in the O^{2-} sublattice to be designated $h^\bullet$ [*Griscom*, 1990]. The $h^\bullet$ are free to roam – as electronic charge carriers – through the oxygen anion sublattice. Therefore, when the peroxy defects break up, releasing $h^\bullet$ charge carriers, the electrical conductivity increases sharply as demonstrated in **Figure 3d**, rising by 6-7 orders of magnitude over a 250°C wide interval, from about 450°C to about 700°C.

Close to 700°C the release of $h^\bullet$ charge carriers comes to completion, marking the end of dissociation of defect **II**. Above 700°C the conductivity drops. The reason is that another process sets in, namely Mg^{2+} diffusion, which becomes thermally activated above ~600°C [*Lempicki*, 1953]. Mg^{2+} diffusion is essential for non-stoichiometric $Mg_{1-\delta}O$ to return to equilibrium. It requires annihilation of the excess Mg^{2+} vacancies at the crystal surface, a process that proceeds by way of cation vacancy hopping [*Conrad and Yang*, 2010; *Sempolinski and Kingery*, 1980; *Wuensch et al.*, 1991].

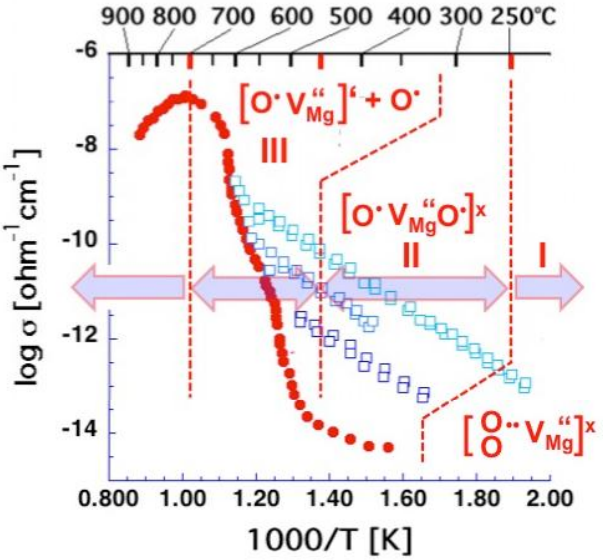

***Figure 4**: Interpretative representation of the anomalous electrical conductivity pattern of highest purity MgO single crystals, supposedly a model insulator. Three temperature windows are identified, below 250°C, between 250-450°C and 450-700°C, each associated with different states of peroxy defects in the MgO matrix, designated as **I**, **II** and **III**. The dissociation of the defect **III** uniquely controls the electric conductivity of MgO through the release of positive hole charge carriers, $h^\bullet$, here shown as $O^\bullet$ states.*

Thermodynamic Equilibrium and Non-Equilibrium Conditions

If O^- is to be introduced into MgO under thermodynamic equilibrium conditions, highly oxidizing conditions are required [*Wuensch et al.*, 1991]. No MgO crystal grown from the melt of a carbon arc fusion furnace under highly reducing conditions should contain oxygen in the valence state 1-. Therefore, the presence of peroxy defects appears to be in disagreement with thermodynamics.

However, the reaction described by eq. [8], the loss of H_2 as described by eq. [9], and the presence of oxygen in the valence 1– are not in conflict with thermodynamics. Nor is the presence of excess Mg^{2+} vacancies in the non-stoichiometric $Mg_{1-\delta}O$. The number of Mg^{2+} vacancies in the MgO matrix is not a reflection of the O_2 fugacity at the time of crystallization but a consequence (i) of the concentration of H_2O dissolved in the MgO matrix under thermodynamic equilibrium conditions and (ii) of the solid state reactions described by eqs. [8] and [9], which occurred at temperatures too low for equilibrium to be maintained.

When nanocrystalline $Mg_{1-\delta}O$ produced by the outdiffusion of H_2 according to eq. [14] was heated above 600°C, atomic O started to evolve, indicating disproportionation [*Martens et al.*, 1976b]:

$$O_2^{2-} \Rightarrow O^{2-} + O \qquad [17]$$

Through this reaction $Mg_{1-\delta}O$ evolves toward the 1:1 stoichiometry that a material like MgO with Schottky defects is supposed to have at thermodynamic equilibrium [*Alfé and Gillan*, 2005]:

$$Mg_{1-\delta}O \Rightarrow MgO + \delta/2\ O_2 \qquad [18]$$

Confirmation of Positive Holes by Dielectric Polarization

Electrical conductivity measurements do not provide the sign of the majority charge carriers. If we want to learn more about the nature of the charge carriers, it is advisable to supplement conductivity measurements with corroborating techniques.

One option is to conduct Hall effect measurements, widely used to study semiconductors [*Clayhold and B. M. Kerns*, 2008], which provide information about the sign of the majority charge carriers and their mobilities. Another option is to measure the dielectric polarization **P**, a fundamental property of materials, given by $\mathbf{P} = \varepsilon_O(\varepsilon-1)/4\pi\ \mathbf{E}_{ext,}$ where ε_0 and ε are the permittivity of vacuum and dielectric constant, respectively, and $\mathbf{E}_{ext}$ is the externally applied electric field [*Freund et al.*, 1989].

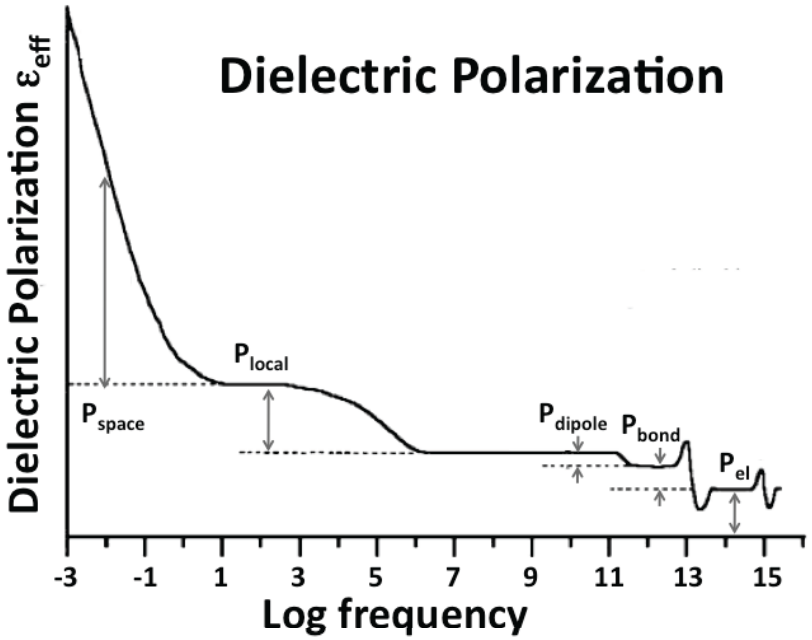

***Figure 5**: Schematic representation of the dielectric polarization of insulators, giving rise to the effective dielectric constant ε_{eff}, a fundamental bulk property. Different contributions are identified. The first three on the right, at high frequencies, are characteristic of perfect crystals. The 4th and 5th arise from defects, which either increase the local polarizability or create mobile charges that can move as a space charge in the externally applied E field.*

As illustrated in **Figure 5** the dielectric polarization $\mathbf{P}_{total}$ is composed of several contributions in different frequency ranges. Five contributions are characteristic of the bulk, $\mathbf{P}_{el}$, $\mathbf{P}_{bond}$, $\mathbf{P}_{dipole}$, $\mathbf{P}_{local}$, and $\mathbf{P}_{space}$, plus a sixth contribution, $\mathbf{P}_{surface}$, which arises from the surface [*Kittel*, 1980]. At high frequencies, in the visible (VIS) region, 10^{15}–10^{13} Hz, only electrons can respond to the rapidly alternating E field. Their contribution $\mathbf{P}_{el}$ defines the refractive index n. In the infrared (IR) region, below 10^{13} Hz, atoms linked by bonds or forming dipoles can follow the E_{ext} field, converting energy into atomic vibrations. The sum ($\mathbf{P}_{el} + \mathbf{P}_{bond} + \mathbf{P}_{dipole}$) defines the dielectric constant, ε, linked to the refractive index n by the Lorentz-Lorenz relation $n = \sqrt{\varepsilon}$. In perfect dielectrics $\mathbf{P}_{total}$ will not increase further with decreasing frequency. In practice defects are always present, some of which may have dipoles that can align in the E_{ext} field, possess a local polarizability that is different from that of the surrounding matrix. Their contributions are combined in $\mathbf{P}_{local}$. When mobile charge carriers appear, they can form space charges that respond to the external E_{ext} field. Their contribution is designated as $\mathbf{P}_{space}$. In the context of this paper only $\mathbf{P}_{local}$ and $\mathbf{P}_{space}$. are of interest.

The sixth contribution, $\mathbf{P}_{surface}$, arises uniquely from the surface. When a dielectric generates mobile charge carriers, these charge carriers repel each other in the bulk and are driven toward the surface. The sign of the surface charge is determined by the majority charge carriers, their number density n

and mobility μ. According to eqs. [5a/b] the surface charge is positive if n'μ' < n•μ•, indicating p-type, and negative, if n'μ' > n•μ• indicating n-type characteristics [King, 1984 #102].

Figure 6 illustrates the principle of the measurement, the protocol and representative results [*Freund et al.*, 1989]. **Figure 6a** shows the sample placed between a small gold sphere and an annular gold electrode. Connecting the annular electrode to ground and applying a voltage to the small electrode, generates a divergent electric field, which produces a force F_z acting on the sample. In practice the sample is suspended from a microbalance into a small, cup-shaped furnace, which contains both electrodes. **Figure 6b** shows a temperature-time program with temperature steps, ΔT, typically in 5° or 10°C increments/decrements. During each ΔT step, at constant T, a voltage-time program is applied as shown in **Figure 6c** with typical ±ΔV steps of ±5, ±10, ±20 or ±50 V.

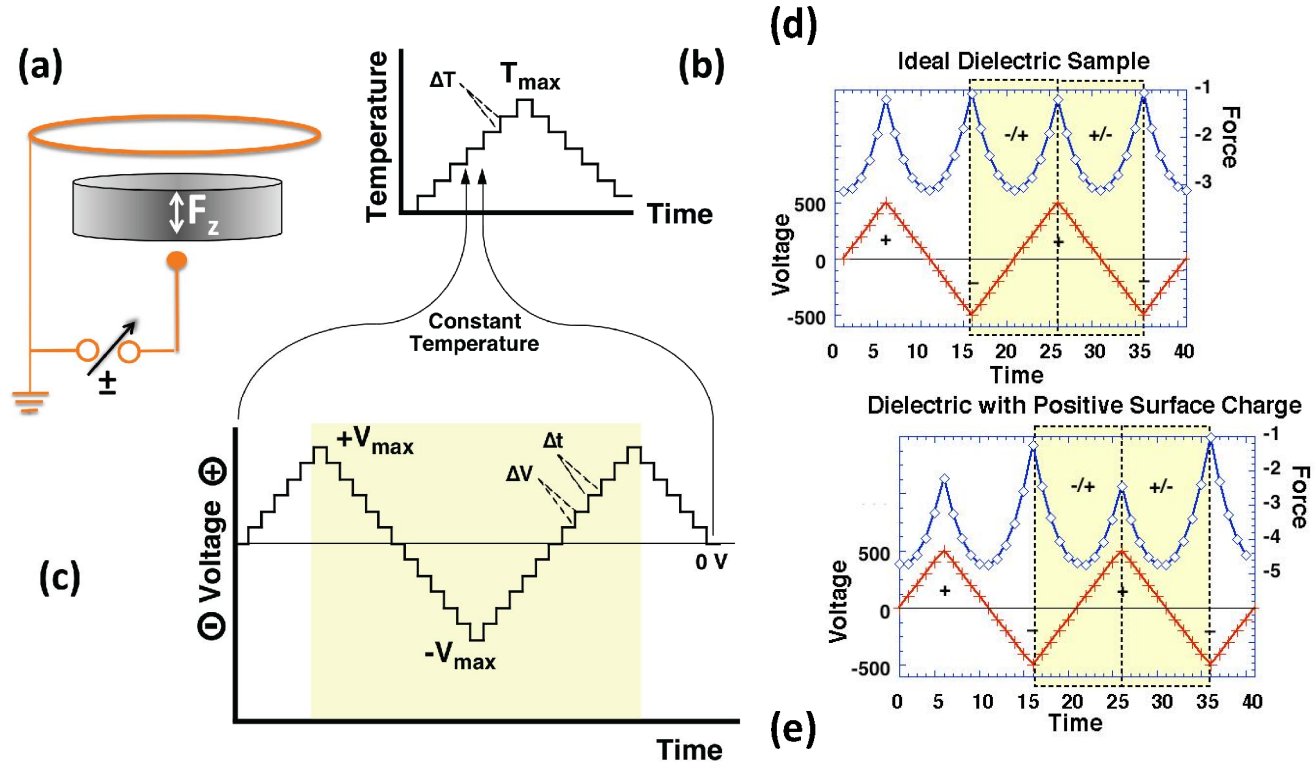

***Figure 6**: Principle and execution of a dielectric polarization measurement in a divergent electric field gradient (see text).*

In the case of a dielectric with contributions from $\mathbf{P}_{el}$, $\mathbf{P}_{bond}$, $\mathbf{P}_{dipole}$, $\mathbf{P}_{local}$, and $\mathbf{P}_{space}$,, F_z is proportional to the square of the applied voltage leading to parabolas as in **Figure 6d**. In the case of a dielectric with mobile positive charges in the bulk, which make a $\mathbf{P}_{surface}$ contribution, the parabolas are skewed by the addition of a linear term, proportional to the density of the surface charge, as illustrated in **Figure 6e**.

Bulk and surface contributions can be separated by forming linear combinations $\mathbf{F}_\Sigma = \frac{1}{2}(\mathbf{F}_z^- + \mathbf{F}_z^+)$ and $\mathbf{F}_\Delta = \frac{1}{2}(\mathbf{F}_z^- - \mathbf{F}_z^+)$, where $\mathbf{F}_z^+$ and $\mathbf{F}_z^-$ are the forces measured with + and – bias, respectively.

$\mathbf{F}_\Sigma$ depends quadratically on the bias voltage and is given by:

$$F_{\Sigma} = -\int_{vol} \{[P_{el} + P_{bond} + P_{dipole} + P_{local} + P_{space}]\nabla\} E_{ext} dV \qquad [19]$$

$\mathbf{F}_{\Delta}$ depends linearly on the bias voltage and is a unique function of the surface charge density:

$$F_{\Delta} = -\int_{v} [P_{surface}\nabla] E_{ext} dV \qquad [20]$$

Figures 7a/b show $\mathbf{F}_{\Sigma}(T)$ and $\mathbf{F}_{\Delta}(T)$ plots of an MgO single crystal, here a 3N-MgO crystal, 99.9% basic purity grade doped with 200 ppm Co^{2+}. $\mathbf{F}_{\Sigma}(T)$ and $\mathbf{F}_{\Delta}(T)$ graphs of undoped 4N-MgO or of moderately doped 3N-MgO crystals with divalent 3d-transition metal cations are practically indistinguishable. The data were obtained during stepwise heating to T_{max}= 600°C in N_2 atmosphere following the protocol depicted in **Figure 6b** with 15 sec polarization time at each ΔV step during each ΔT step. The dotted line in **Figure 7a** indicates how $F_{\Sigma}(T)$ changes, if the polarization time is 15 min at each ΔV step. The 15 min polarization data were obtained in a separate run over this narrow T interval. **Figure 7b** indicate the evolution of $F_{\Delta}(T)$. The black triangles show F_{Δ} going negative, if heating is continued above 600°C. These data were obtained in a separate run.

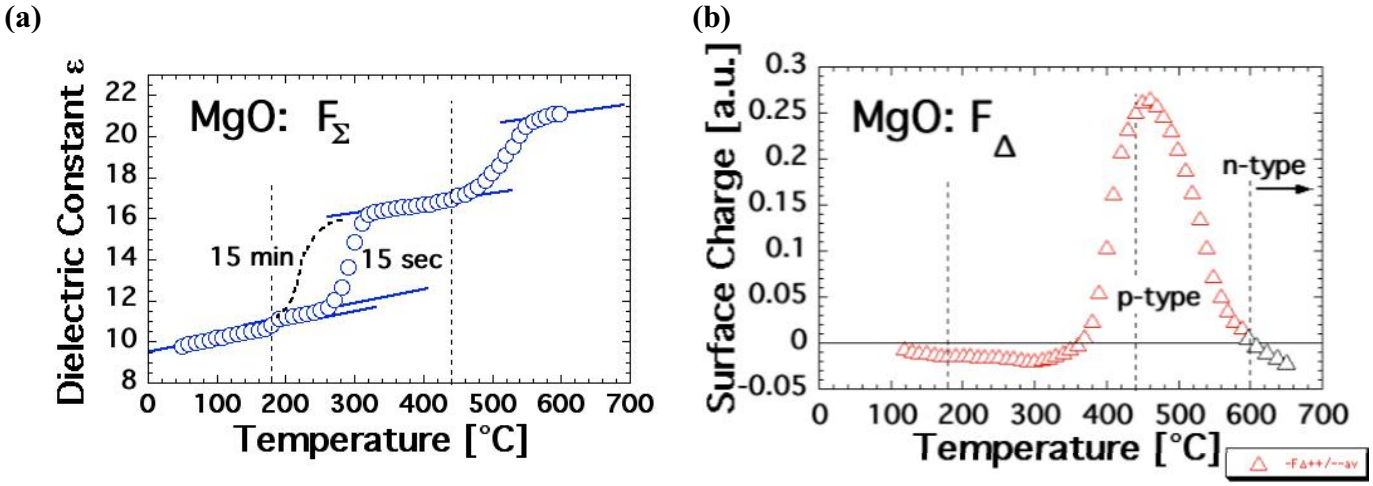

***Figure 7a/b**: Bulk polarization F_{Σ} and surface charge F_{Δ} show the evolution of the effective dielectric constant and the thermal activation of positive charge carriers in MgO during heating to 600°C, which is consistent with the 2-step activation process as described by eqs. [15/16].*

In **Figure 7a** the $F_{\Sigma}(T)$ data are fitted to the dielectric constant ε of MgO, 9.6 at room temperature [*Young and Frederikse*, 1973]. At the limit of 0 Hz ε begins to increase around 250°C at 15 sec polarization time or already around 200°C at 15 min polarization time. ε reaches a plateau around 350°C but exhibits a second stepwise increase beginning around 450°C. The $F_{\Delta}(T)$ data in **Figure 7b** indicate a slightly negative surface charge of the MgO up to about 350°C, followed by a pronounced positive surface charge, indicating the onset of p-type behavior. The positive surface charge reaches a maximum about 450°C, then decreases and turns negative above 600°C, indicating n-type behavior.

According to eq. [14] $F_{\Sigma}(T)$ is the sum of the five bulk contributions to $\mathbf{P}_{total}$. Only the last two, $\mathbf{P}_{local}$ and $\mathbf{P}_{space}$, depend on the presence of defects. The stepwise increase in $F_{\Sigma}(T)$ indicates that these defects are thermally activated. During the first increase, there is no change in $F_{\Delta}(T)$, i.e. no activation of mobile charge carriers. This means that the first $F_{\Sigma}(T)$ increase, which begins at 250°C or 200°C, is due to the thermal activation of defects, which only affect the local polarizability, $\mathbf{P}_{local}$.

This is fully consistent with the transition of the tightly bound, spin-coupled peroxy defect $[^{O}_{O}\bullet\bullet V''_{Mg}]^{x}$, designated state **I**, to state **II**, the spin-decoupled state $[O^{\bullet} V''_{Mg} O^{\bullet}]^{x}$ as described by eq. [10]. It is consistent with the absence of any significant increase in the electrical conductivity of the MgO in the temperature range below approximately 350°C as evidenced in **Figure 3a**.

By contrast, above 350°C, the electrical conductivity of the MgO starts to increase as shown in **Figure 3a**, indicating the activation of mobile charge carriers. This is consistent with the increase in $F_{\Sigma}(T)$, due to a contribution of $\mathbf{P}_{space}$ and simultaneous $\mathbf{P}_{surface}$ contribution as reflected in the change in $F_{\Delta}(T)$ in **Figure 7b**. This is consistent with the break-up of the peroxy bond as described by eq. [11], i.e. with the transition of the spin-decoupled state $[O^{\bullet} V''_{Mg} O^{\bullet}]^{x}$ to the dissociated state $[O^{\bullet} V''_{Mg}]' + O^{\bullet}$ and the activation of mobile positive hole charge carriers $h^{\bullet}$.

Dielectric polarization measurements during cooling show that $F_{\Sigma}(T)$ is fully reversible under the conditions of the experiments, i.e. under slow stepwise cooling over many hours. The high temperature portion of $F_{\Delta}(T)$, the trend from the high positive values around T_{max} ~500°C toward negative values at ~600°C, is also reversible. Below ~500°C, however, the surface charge lingers on, causing $F_{\Delta}(T)$ to remain positive down to ambient temperatures. At room temperature the surface charge dissipates over the course of hours with about the same time constant with which the electrical conductivity $\sigma(T)$ recovered during annealing as discussed in the context of **Figures 3a-c**.

Positive Hole Charge Carrier Activation in Feldspars

MgO is not the only material that contains peroxy defects and activates positive hole charge carriers at distinct temperature steps upon heating. Silicates also contain peroxy defects, probably in the form of peroxy bridges, $O_3Si^{/OO\backslash}SiO_3$ or $O_3Si^{/OO\backslash}AlO_3$, replacing $O_3Si^{/O\backslash}SiO_3$ or $O_3Si^{/O\backslash}AlO_3$ bonds respectively, or linking $[SiO_4]$ groups.

In the case of MgO the introduction of peroxy defects was linked to the dissolution of H_2O and formation of hydroxyl pairs associated with Mg^{2+} vacancies, OH^{-}, followed by the redox conversion described by eqs. [13/14]. Feldspars are tectosilicates the structures of which consist of $[Si,AlO_4]$ tetrahedra 3-dimensionally connected by $O_3Si^{/O\backslash}SiO_3$ and/or $O_3Si^{/O\backslash}AlO_3$ bonds. If H_2O is dissolved, it will most likely hydrolyze the bonds forming as primary product hydroxyl pairs:

$$O_3Si^{/O\backslash}SiO_3 + H_2O \quad \Leftrightarrow \quad O_3Si^{/OH}{}_{HO/}SiO_3 \qquad [21]$$

The hydroxyl pair on the right hand side of eq. [21] could undergo the same type of redox conversion as OH^{-} pairs in MgO, leading to"

$$O_3Si^{/OH}{}_{HO/}SiO_3 \quad \Leftrightarrow O_3Si^{/OO\backslash}SiO_3 + H_2 \qquad [22]$$

Feldspars indeed exhibit the same $F_{\Sigma}(T)$ and $F_{\Delta}(T)$ behavior when heated. This is exemplified in **Figure 8a/b** for $F_{\Sigma}(T)$ of a sanidine single crystal from Volkesfeld, Eifel volcanic district, Germany [*Bertelmann et al.*, 1985], and for $F_{\Sigma}(T)$ of an anorthosite from Larvik, Norway [*Wanvik*, 2000]. The sanidine, $K_{0,96}Na_{0,14}AlSi_3O_8$, was cut from a very large (40 cm) single crystal extracted from a leucite phonolite tuff [*Bank*, 1967]. The anorthosite sample consisted of an 8 mm diameter disk, 2 mm thick, cut of the coarsely polycrystalline Larvik anorthosite rock. The sanidine and anorthosite were transparent or translucent and smoky gray due to the presence of unbound positive holes, which localize at low temperatures at $O_3Si^{/O\backslash}AlO_3$ or $O_3Al^{/O\backslash}AlO_3$ [*Speit and :ehmann*, 1982]. Both bleached

upon heating beyond 500°C to a light gray color.

In both cases $F_\Sigma(T)$ increases in 2 steps, at 200-250°C and 400-500°C for the sanidine and at 100-150°C and 400-500°C for the anorthosite. The $F_\Delta(T)$ response, which is not shown, is somewhat complicated by the fact that the unbound positive holes anneal out during first heating. Therefore a stable $F_\Delta(T)$ response can be obtained only after careful annealing during second and subsequent heating cycles [unpubl. results].

(a) **(b)**

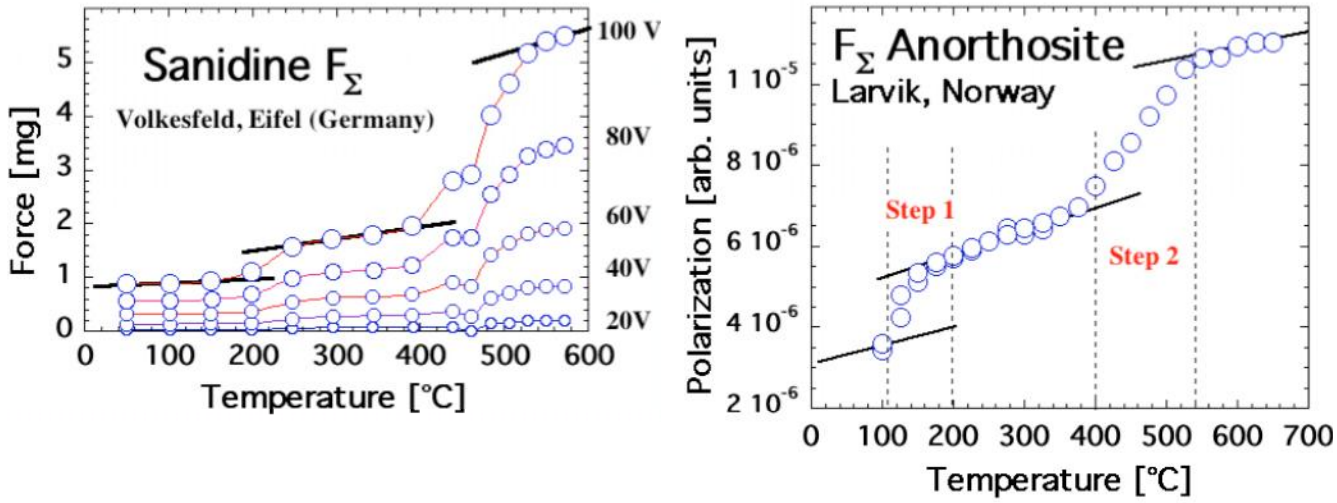

***Figure 8a**: $F_\Sigma(T)$ of a sanidine single crystal from Volkesfeld, Eifel volcanic field, brought up by an explosive eruption producing a leucite phonolite tuff [Bank, 1967]. The $F_\Sigma(T)$ response as measured at different voltages is shown. **Figure 8b**: $F_\Sigma(T)$ of a coarsely crystalline anorthosite from Larvik, Norway [Wanvik, 2000]. Both feldspar specimens exhibit the characteristic $F_\Sigma(T)$ behavior that points to the presence of peroxy defects and their 2-step activation, leading to the release of positive hole charge carriers.*

The similarity of the $F_\Sigma(T)$ response of sanidine and anorthosite to the $F_\Sigma(T)$ response of MgO is striking. Since we know for certain that, in the case of MgO, the 2-step increase in $F_\Sigma(T)$ is due to the 2-step break-up of peroxy defects in the MgO matrix and activation of positive hole charge carriers, we take the results presented in **Figure 8a/b** as indication that these feldspars also contain peroxy defects.

If this is so, the question arises whether there are other materials, compositionally similar to feldspars, which are produced under conditions that are not conducive to the introduction of "water" in form of solute O_3Si-OH. Normal plate glass, produced from the melt at relatively low temperature and low relative humidity levels, is such a material. Typical compositional ranges of clear glasses in mol-% are SiO_2 63-81, Al_2O_2 0-2, MgO 0-6, CaO 7-14, Na_2O 9-15, K_2O 0-1.5 with most others below 0.5%.

Figure 9a/b show the $F_\Sigma(T)$ and $F_\Delta(T)$ responses of plate glass heated to 500°C. $F_\Sigma(T)$ exhibits a increasing trend consistent with the increase in the overall polarizability as a function of temperature. At the glass transition temperature T_g $F_\Sigma(T)$ increases more sharply, due to an increase in $\mathbf{P}_{local}$ as a result of the softening of the glass structure and increase in diffusivity of Na^+ and other alkali cations. $F_\Sigma(T)$ is mostly reversible under the conditions of the experiment with some hysteresis during cooling below T_g. The reason for the slight deviation from a linear $F_\Sigma(T)$ increase/decrease around 200°C is

unknown. However, the overall $F_\Sigma(T)$ response of the glass is distinctly different from the $F_\Sigma(T)$ behavior of either feldspar minerals shown in **Figure 8a/b**. There is no evidence for the characteristic $F_\Sigma(T)$ response linked to the 2-step activation of peroxy defects.

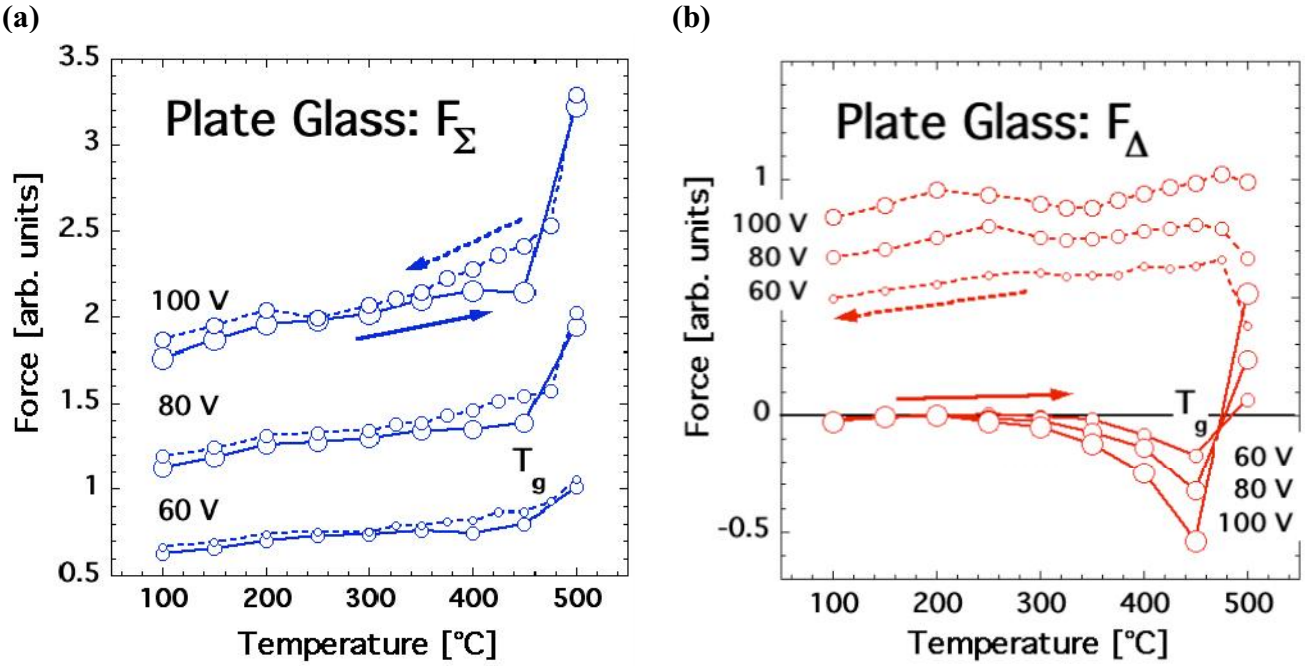

***Figure 9a/b**: Dielectric polarization response of common plate glass provides no evidence for peroxy defects and the thermal activation of positive hole charge carriers.*

This conclusion is supported by the $F_\Delta(T)$ response shown in **Figure 9b**. During heating a slight negative surface charge develops, which changes abruptly to a positive surface charge above T_g. The evolution of $F_\Delta(T)$ towards positive values is due to the high diffusivity of Na^+ and other alkali cations in the externally applied divergent E field. The Na^+ segregation is irreversible during cooling down to room temperature as demonstrated by the persistence of the positive $F_\Delta(T)$ values in **Figure 9b**.

The absence of evidence for peroxy defects in the dielectric polarization response of normal plate glass is consistent with the overall theme of this study: Peroxy defects are formed metastably out of solute OH^-, O_3Si-OH, or O_3Al-OH, presumably hydroxyl pairs, which undergo a redox conversion during cooling. This reaction takes place in glasses as well as in crystalline materials. For instance, fused silica, which dissolves traces of H_2O at a much higher temperature than ordinary plate glass, has been shown to contain peroxy defects and activated positive hole charge carriers in much the same way as melt-grown MgO [*Freund and Masuda*, 1991].

Peroxy Defects and Positive Hole Charge Carrier Activation in Olivine

The dielectric polarization behavior described in the preceding section indicates the thermal activation of mobile positive hole charge carriers in MgO and feldspar crystals but not in regular plate glass. It provides unambiguous support for the presence of peroxy defects in MgO grown from the melt under the extremely reducing conditions of a carbon-arc fusion furnace [*Abraham et al.*, 1971] and in feldspar specimens that crystallized in a magma under reducing lower crustal conditions. The dielectric polarization response is fully consistent with the electrical conductivity behavior of the melt-grown MgO and magma-grown feldspar crystals. It is fully consistent with our conclusion from the

589 first part of this paper that positive hole are the controlling charge carriers that define the electrical
590 conductivity in the LT region, up to about 600°C, of MgO and of mafic and ultramafic rocks.

591 This study points to a mechanism by which crystals grown under reducing, even extremely reducing
592 conditions, can acquire excess oxygen in the form of peroxy defects. The peroxy defects are
593 introduced via the dissolution of H_2O. The dissolution of H_2O, however, is a process that is very
594 common in nature. It takes place whenever minerals and rocks crystallize from an H_2O-laden magma.

595 The electrical conductivity of dunite, an olivine-rich peridotite, is illustrated in **Figure 10**, adapted
596 from work by Constable and Duba [*Constable and Duba*, 1990]. During heating in a 1:1 $CO:CO_2$
597 atmosphere, the conductivity increases rapidly between ~350°C and 670°C. At 670°C, as T was held
598 constant for an unspecified length of time, the conductivity decreased precipitously. During further
599 heating the conductivity increased again, merging into a high temperature branch similar to the HT
600 branch observed with MgO. During cooling the beginning of an Arrhenius straight section can be seen
601 with an activation energy of ~1 eV characteristic of the LT conductivity response of MgO.

602 The interpretation given by Constable and Duba [*Constable and Duba*, 1990] is based on the
603 assumption that, during heating, carbon was depositing out of the vapor phase onto the sample surface,
604 providing a low resistivity pathway. The carbon deposition is assumed to have ended at 670°C when,
605 according to thermodynamic calculations, the 1:1 $CO:CO_2$ mixture was leaving the stability field of
606 graphite, creating oxidizing conditions, which caused the surface carbon film to "burn off".

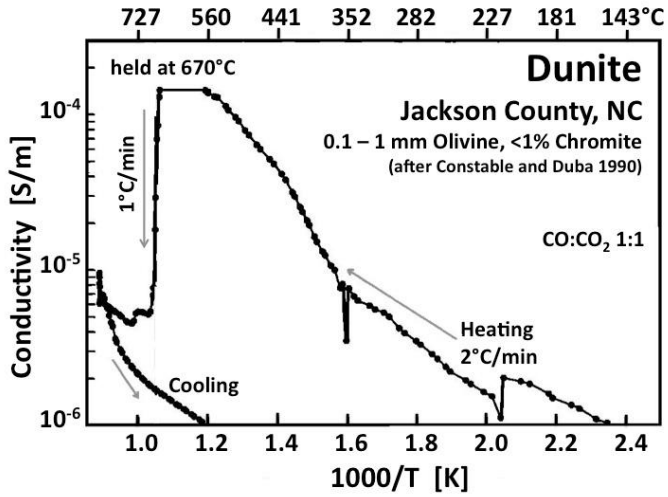

***Figure 10**: Electrical conductivity measured on a sample of Jackson County peridotite, 99% olivine, in a 1:1 $CO:CO_2$ atmosphere showing an anomalously high conductivity in the LT region, thought to be due to vapor-phase deposited surface carbon (after [Duba and Constable, 1993]).*

607 The comparison between electrical conductivity and dielectric polarization shows that $\mathbf{P}_{total}$ and its
608 separation into $\mathbf{P}_{bulk}$ and $\mathbf{P}_{surface}$ can provide unique information about the nature of the charge carriers
609 responsible for the conductivity response. We therefore present next the dielectric polarization
610 response of an olivine single crystal. To circumvent complications arising from carbon precipitation in
611 the graphite stability field we chose to conduct the first set of experiments in high purity N_2. The
612 choice of an inert gas atmosphere is justified on the basis of the observation that the $CO:CO_2$ = 1:1
613 mixture remained unequilibrated up to at least 500°C, possibly higher [*Constable and Duba*, 1990].

614 The sample was prepared by cutting a 1 mm thick slice, 8 mm diameter, from a randomly oriented
615 cylinder of a gem-quality San Carlos olivine single crystal, 7 mm thick, polished on both sides. Before
616 the slice was cut off, the IR spectrum was recorded.

617 As shown in **Figure 11** the broad absorption in the spectral range of the ν_{OH} stretching vibrations,
618 3150-3700 cm^{-1}, lacks distinct features except for a weak band at 3600 cm^{-1}. The absence of ν_{OH}

bands is conventionally interpreted to mean that such an olivine crystal without OH^- has a very low solute "water" content and may have come from a "dry" of the upper mantle [*Khan and Shankland*, 2011a]. However, there is also the possibility that, similar to OH^- pairs in MgO, solute OH^- in olivine may have converted to H_2 plus peroxy defects. In this case the near-absence of ν_{OH} bands may mean that an olivine crystal with an IR spectrum as exemplified in **Figure 11** may have lost most of its solute OH^- content due to this redox conversion. If the solute OH^- content was originally high, the olivine should have a high concentration of peroxy defects. Measuring the dielectric polarization would then be the technique of choice [*Freund et al.*, 1989].

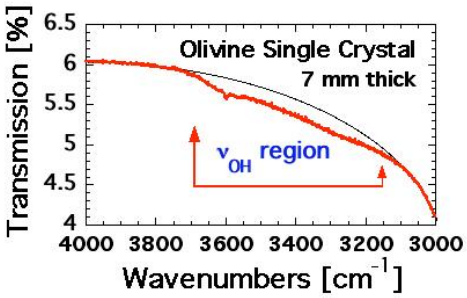

***Figure 11**: Infrared spectrum of a 7 mm thick section of a gem-quality olivine single crystal in the range of the O–H stretching frequencies indicates an extremely low solute OH^- content.*

Figures 12a/b show $F_\Sigma(T)$ and $F_\Delta(T)$ of this olivine crystal, recorded according to the protocol outlined in **Figure 5** with 15 sec polarization time at each ΔT and ΔV step. $F_\Sigma(T)$ is fitted at room temperature to a dielectric constant ε scale. Because the orientation of the olivine single crystal disk is not known, we chose for the one-point fit the average of the three components of the dielectric constant along the crystallographic axes a, b, and c of forsterite [*Cygan and Lasaga*, 1986].

(a) **(b)**

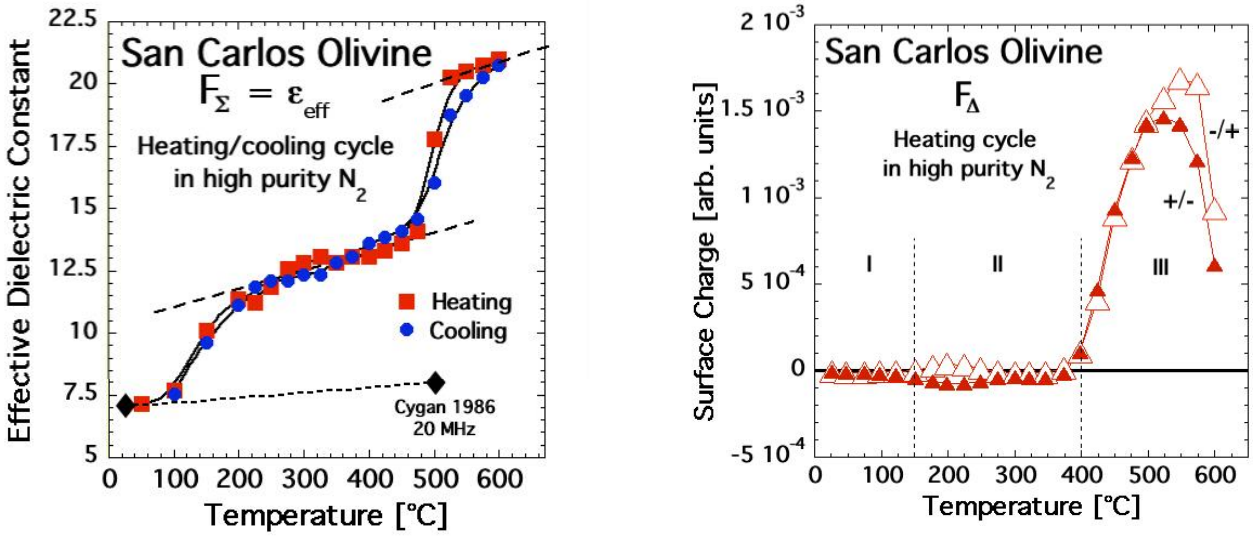

***Figure 12a/b**: Bulk polarization F_Σ and surface charge F_Δ parameters of a San Carlos olivine single crystal, which show that, despite the chemical complexity of this mineral, its effective dielectric constant increases upon heating in the same way as that of high purity MgO, in two distinct steps, and a positive charge appears around 400°C.*

$F_\Sigma(T)$ of this olivine crystal is strikingly similar to $F_\Sigma(T)$ of MgO and of the two feldspar specimens. During heating the bulk polarization increases in a stepwise fashion at 100-250°C and 450-500°C. During cooling $F_\Sigma(T)$ follows closely the heating curve down to at least 100°C.

$F_\Delta(T)$ recorded is also strikingly similar to $F_\Delta(T)$ of MgO and the feldspars. The curves labeled +/- and -/+ correspond to F_Δ values obtained during heating taking the data from the sections going in ΔV steps from +500 V to –500 V and from –500 V to +500 V, respectively. The differences between the two $F_\Delta(T)$ curves provides information about the time-dependent polarization during the 15 sec time steps. $F_\Delta(T)$ remains close to zero from 100°C to almost 400°C, while $F_\Sigma(T)$ goes through its first stepwise increase. Thus the first $F_\Sigma(T)$ increase is due to a $\mathbf{P}_{local}$ contribution to $\mathbf{P}_{bulk}$, without activation of mobile charge carriers. Mobile charge carriers only appear upon approaching 400°C. At first their number is small, insufficient to cause a noticeable increase in $F_\Sigma(T)$. By about 450-500°C their number has increases enough so that $F_\Sigma(T)$ also increases, due to a $\mathbf{P}_{space}$ contribution to $\mathbf{P}_{bulk}$. The sign of the mobile charges in the olivine is unambiguously positive, as in MgO and the feldspar specimens, providing firm evidence that positive holes are the active charge carriers.

Metastability and Thermodynamic Equilibrium

The very weak IR absorption of a 7 mm thick olivine crystal in the range of ν_{OH} stretching vibrations as evidenced by **Figure 11** indicate a near-complete absence of solute OH^-. The same olivine crystal however provides evidence for positive hole charge carriers that become thermally activated at about the same temperature at which positive holes are activated in MgO, suggesting that they derive from peroxy defects in the olivine matrix, formed by the same type of redox conversion that turned OH^- in MgO into $O_2^{2-} + H_2$ as given by eq. [13]. For olivine we have:

$$O_3Si/^{OH}\#_{HO}/SiO_3 \Leftrightarrow O_3Si/^{OO}\backslash SiO_3 + H_2 \qquad [23]$$

where the # sign is used to indicate a divalent cation vacancy, Mg^{2+} or Fe^{2+}.

By analogy to the dilute solid solution MgO–H_2O, we formulate a dilute olivine–H_2O solid solution as:

$$(Mg,Fe^{2+})_2SiO_4 + \delta\, H_2O \Leftrightarrow (Mg,Fe^{2+})_{2-\delta}SiO_{4-2\delta}OH_{2\delta} \qquad [24]$$

If the OH^- in this olivine–H_2O solid solution undergo a redox conversion according to eq. [23] and if some or all of the molecular H_2 is lost from the crystal matrix by outdiffusion, we have:

$$(Mg,Fe^{2+})_{2-\delta}SiO_{4-2\delta}OH_{2\delta} \Leftrightarrow (Mg,Fe^{2+})_{2-\delta}SiO_4 + \delta\, H_2 \qquad [25]$$

where we do not separately indicate on the right hand side the fraction of oxygen in the valence 1–. We specify, however, that the iron continues to be ferrous, Fe^{2+}. In order for the cation-deficient olivine on the right hand side to be balanced, a 2δ fraction of the oxygens have to be in the valence 1–.

Low solute OH^- concentrations are usually interpreted to mean that such crystals come from "dry" regions of the upper mantle [*Bell and Rossman*, 1992; *Miller et al.*, 1987; *Rossman*, 1996]. Eq. [25] suggests instead that solute OH^- may have "disappeared" from the IR spectra by converting to H_2 plus peroxy. Molecular H_2, if present, has an extremely weak $\nu_{H\text{-}H}$ absorption [*Kriegler and Welch*, 1968]. Other techniques such as SIMS or nuclear reaction profiling, which measure the total H concentration, often yield higher H values than those obtained by IR measurements of ν_{OH} [*Bell et al.*, 2003].

"Burning off" Positive Holes in Olivine

If the enhanced electrical conductivity observed during initial heating were due to carbonaceous films precipitated within the stability field of graphite [*Constable and Duba*, 1990], such films should "burn

678 off' under oxidizing conditions. If the enhanced electrical conductivity is due to $h^{\bullet}$, i.e. highly
679 oxidizing O^{-} in a matrix of O^{2-}, the best way to annihilate them is to use reducing conditions.

680 We therefore conducted a dielectric polarization experiment with a San Carlos olivine single crystal,
681 heating it first in pure N_2 atmosphere in 20 temperature steps from 50°C to 600°C, cooled it back in
682 the same steps, and let is sit overnight in the pure N_2. $F_{\Sigma}(T)$ as recorded during this first heating is
683 shown by the top curve labeled with squares in **Figure 13a**.

684 Next we replaced the N_2 with a 9:1 N_2–CH_4 gas mixture and reheated the same olivine crystal five
685 times. The 1st heating in N_2–CH_4, up to 575°C, produced the $F_{\Sigma}(T)$ curve marked by open circles in
686 **Figure 13a**. After stepwise cooling the olivine crystal was reheated in the same N_2–CH_4 gas mixture
687 four more times. The 3rd heating up to 550°C produced the $F_{\Sigma}(T)$ curve shown in **Figure 13a** by open
688 triangles. The 5th heating up to 600°C produced the $F_{\Sigma}(T)$ curve in **Figure 13a** marked by diamonds.

689 **Figure 13b** shows $F_{\Delta}(T)$ curves recorded during the 1st heating in the N_2-CH_4 gas mixture with ± bias
690 voltages of 20V, 40V, 60V and 80V. The $F_{\Delta}(T)$ response displays the same overall pattern as observed
691 for MgO and the feldspar specimens. The dashed lines present the $F_{\Delta}(T)$ response during stepwise
692 cooling: fully reversible from 600°C to about 500°C, followed by elevated $F_{\Delta}(T)$ values below 400°C
693 due to the fact that, after heating in the N_2-CH_4 mixture, the positive surface charge no longer
694 dissipates after cooling.

695 Comparing the $F_{\Sigma}(T)$ response during the 1st run in pure N_2 and the subsequent runs in the N_2–CH_4 gas
696 mixture provides insight into the reactions at the olivine surface. **Figure 13a** shows that, during
697 heating in the presence of CH_4, the $F_{\Sigma}(T)$ response is similar up to about 450°C, though the values are
698 slightly lower. This overall decrease of $F_{\Sigma}(T)$ is due to the fact that the 1st heating in pure N_2 had
699 already caused changes in the polarization response of the olivine, presumably due to oxidation of Fe^{2+}
700 to Fe^{3+} in the olivine matrix, equivalent to the annihilation of mobile $h^{\bullet}$ charge carriers.

701 Above 450°C the $F_{\Sigma}(T)$ curve drops during heating in the N_2–CH_4 gas mixture, indicating that $h^{\bullet}$
702 charge carriers are being consumed. Above 530°C $F_{\Sigma}(T)$ increases again, indicating that the surface
703 reaction, which consumes $h^{\bullet}$ charge carriers, has stopped and new $h^{\bullet}$ are able to flood the surface. This
704 behavior, in particular the dip of $F_{\Sigma}(T)$ above 450°C, repeats itself during the 3rd heating cycle. By the
705 time of the 5th heating, however, the dip has essentially disappeared, indicating that the reaction
706 between the olivine and CH_4 has reached some form of endpoint.

707 Of further interest is the fact that, in the ΔT range marked in pale yellow in **Figures 13a/b**, $F_{\Sigma}(T)$
708 continues to increase even though the $F_{\Delta}(T)$ curves show that $h^{\bullet}$ charge carriers have already begun to
709 flood the olivine surface. $F_{\Sigma}(T)$ begins to dip in the ΔT range marked in yellow, i.e. only after the
710 $F_{\Delta}(T)$ values have reached their maxima. The area marked in red outlines the ΔT range, where $F_{\Sigma}(T)$
711 recovers, rising in spite of the presence of CH_4.

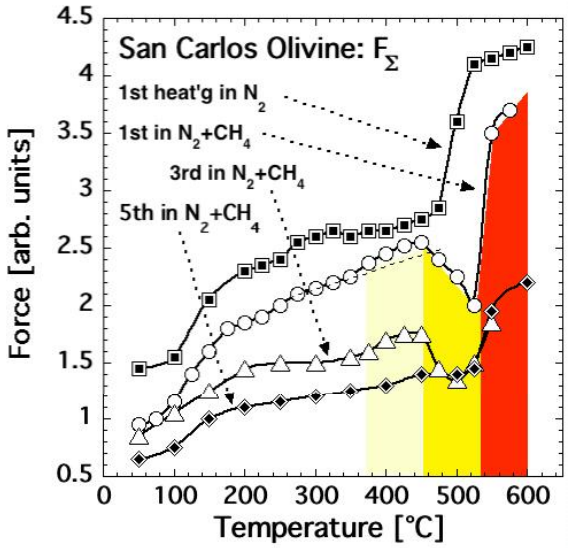

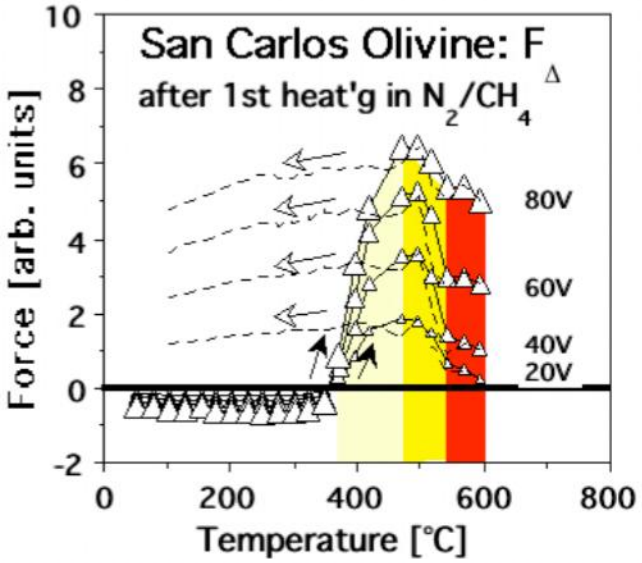

Figure 13a: *Bulk dielectric polarization of an olivine crystal subjected to 6 heating /cooling cycles, the 1st in pure N_2, the others in N_2–CH_4 gas mixtures. The colors indicate temperature regions at which $h^\bullet$ become activated but do not yet react with the CH_4 (light yellow), start to react with the CH_4 (yellow), and overwhelm the reaction with CH_4 (red)*

Figure 13b: *Surface charge developing on an olivine crystal during the 1st heating/cooling in the N_2–CH_4 gas mixture. In contrast to the first heating in pure N_2, when the positive surface dissipates after cooling, heating in the N_2–CH_4 gas mixture leaves a positive surface charge. The colors correlate with ΔT ranges at which the bulk polarization of the olivine crystal is affected by the reaction with CH_4.*

Summarizing this last set of experiments we can say with additional confidence that, though the olivine crystals under study have originated in the upper mantle and crystallized in a highly reducing environment, they release highly oxidizing $h^\bullet$ charge carriers upon heating. From this we infer that they contain peroxy defects, presumably formed during cooling by way of a redox conversion of OH^- pairs that had been incorporated into the olivine structure at upper mantle temperature through dissolution of traces of "water". Consistent with our earlier conclusion that $h^\bullet$ are highly oxidizing O^-, they are consumed by a reaction with CH_4, presumably through oxidative coupling, which produces OH^- and methyl as an intermediate, $\bullet CH_3$ [*Asame et al.*, 1988].

Discussion

In this paper we have focused on fundamental processes that are important for understanding the electrical properties of materials, both laboratory-grown and from natural environments, both single crystal minerals and igneous rocks. We make the extraordinary claim that MgO crystals, grown from the melt under the viciously reducing conditions of a carbon arc fusion furnace, contain peroxy defects in their crystal structure, hence oxygen in the oxidized valence state 1–. When the peroxy defects break up, they release positive hole charge carriers, formally defect electron in the oxygen anion sublattice, equivalent to O^- in a matrix of O^{2-}. These positive holes have two outstanding properties: they are highly mobile and highly oxidizing.

We make the even more extraordinary additional claim that olivine crystals, which have been brought up from the upper mantle, feldspar crystals, which have been brought up from the lower crustal depth,

and – more generally – mafic/ultramafic rocks such as basalts, gabbro and peridotite produce the same type of mobile positive hole charge carriers and, hence, must also contain peroxy defects. This claim seems to run counter to the well-established fact that upper mantle and lower crustal environments are highly reduced and highly reducing. Thermodynamically, oxygen in the oxidized valence state 1– can never be introduced under these *in situ* conditions.

In fact there is no contradiction with thermodynamics. The reason is that the process, which occurs under *in situ* conditions, is the dissolution of H_2O into the matrix of MgO grown from the carbon arc fusion melt and into the matrix of silicates crystallizing from a magma. The dissolution of H_2O and formation of solute OH^- or $O_3Si\text{-}OH$ are redox insensitive. They can occur irrespective of the redox state of the system. According to our results O^- is introduced through a follow-on process, the redox conversion of hydroxyl pairs to peroxy defects plus H_2. This process only occurs under metastable conditions, namely during cooling when the systems have drifted out of thermodynamic equilibrium.

Depending upon the rate at which a rock or a crystal is cooled, thermodynamic equilibrium can only be maintained as long as diffusional processes remain thermally activated. Diffusional processes are necessary for the adjustment of the oxidations states of transition metal cations and the adjustment of the cation vacancy concentration, both dictated by the oxygen fugacity of the system. Without these continuous adjustments any system will be out of thermodynamic equilibrium. Even at very slow cooling rates these diffusional processes become so slow around 600°C that they can be considered frozen[2]. At faster cooling rates the freezing temperatures tend to be higher, more in the 700°C range.

The *in situ* redox conversion, which turns solute hydroxyl pairs into peroxy defects plus molecular H_2, takes place below 600°C, in the 600-400°C window, when the systems under consideration – MgO, feldspar, olivine crystals and igneous rocks – have already drifted out of thermodynamic equilibrium. Since the redox conversion as outlined by eqs. [13] and [23/25] operate outside equilibrium, oxygen in the valence 1– can exist metastably in an otherwise reduced environment and can co-exist with reduced cations such as Fe^{2+}. Since O^- form highly mobile electronic charge carriers, the electrical conductivity behavior is affected.

Therefore, the claim of oxygen in the valence state 1– is not as extraordinary as it may first appear. The presence of O^- does not contradict thermodynamics because, by the time O^- is introduced, equilibrium thermodynamics is no longer in control. The work presented here casts doubts on the validity of the widely offered explanation of thin carbonaceous films deposited from CO/CO_2-laden fluids in the crust [*Glover and Vine*, 1992; *Shankland et al.*, 1997] and upper mantle [*Constable and Duba*, 1990; *Duba and Constable*, 1993; *Mathez*, 1987; *Roberts et al.*, 1999]. Maybe electrolytically conductive, intergranular fluids and/or intergranular carbonaceous films are not needed to explain the origin of zones of high electrical conductivity in the lower continental crust, which have been called "a long-standing mystery" [*Frost et al.*, 1989]. Those high conductivity zones, which have been identified by magneto-telluric sounding techniques, appear to be an almost universal feature of the Earth's crust at a depth range of about 20 km [*Glover*, 1996; *Lee et al.*, 1983; *Qin et al.*, 1992].

If peroxy defects and thermally activated positive hole charge carriers can be metastably present, we can tie the high conductivity zones to the geotherm [*Freund*, 2003]. If temperatures along the geotherm reach values sufficiently high to thermally dissociate peroxy defects and release positive hole charge carriers, we can envision a depth range, where the peroxy defects would be in a permanently dissociated state. With reference to eq. [7] this means an increase in the number density n of mobile charge carriers and, hence, an increase in the conductivity σ. Deeper into the crust, at

774

[2] This statement holds for "dry" systems. In environments with free supercritical fluids and other fluid-dominated systems equilibrium can be established down to lower temperatures.

higher temperatures, the positive holes will be consumed by equilibrium oxidation reactions, for instance Fe^{2+} to Fe^{3+}, concomitant with structural rearrangements that require cation and cation vacancy diffusion to be thermally activated.

An analogous situation is seen in the experimental conductivity curves obtained during heating of MgO single crystals as depicted in **Figures 3a**, **3c**, and **3d**: at temperatures above 500-700°C the electrical conductivity decreased precipitously because the $h^{\bullet}$ charge carriers begin to be consumed by reactions linked to the return of the MgO crystals toward equilibrium. The same behavior is reflected in the conductivity curve recorded during heating of an olivine single crystal as depicted in **Figure 9**, even though the authors of this graph base their interpretation of the conductivity decrease at 630°C on the assumption that vapor-phase deposited carbon films on the sample surface where "burning away" as the system moved out of the stability field of graphite in the $CO:CO_2$ gas mixture [*Constable and Duba*, 1990]. Finally, the dielectric polarization behavior of the olivine single crystal heated in a $CO:CH_4$ gas mixture as depicted in **Figure 13a/b** indicates as well that $h^{\bullet}$ charge carriers are being consumed under highly reducing conditions – in this case by reacting with CH_4 by way of an oxidative coupling that produces OH^- and methyl as an intermediate, $\bullet CH_3$ [*Asame et al.*, 1988].

References

Abraham, M. M., et al. (1971), Growth of high-purity and doped alkaline earth oxides; PartI: Magnesium oxide and calcium oxide., *J. Chem. Phys.*, *55*, 3752-3756.

Alfé, D., and M. J. Gillan (2005), Schottky defect formation energy in MgO calculated by diffusion Monte Carlo, *Phys. Rev. B*, *71*, 220101.

Asame, K., et al. (1988), Selective oxidative coupling of methane to ethane and ethylene., in *Methane Conversion*, edited by D. M. Bibby, et al., pp. 403-407, Elsevier Publ., Amsterdam.

Bai, L.-P., et al. (2002), The experimental studies on electrical conductivities and P-wave velocities of anorthosite at high pressure and high temperature, *Acta Seismologica Sinica*, *15*(6), 667=676.

Bank, H. (1967), Hellbrauner klar durchsichtiger Alkalifeldspat von Volkesfeld, Eifel, *Zeitschrift Deutsche Gesellschaft Edelsteinkunde*, *61*, 50-53.

Batllo, F., et al. (1991), Positive hole centers in magnesium oxide — correlation between magnetic susceptibility, dielectric anomalies and electric conductivity., *J. Appl. Phys.*, *69*, 6031-6033.

Bell, D. R., and G. R. Rossman (1992), Water in earth's mantle: The role of nominally anhydrous minerals., *Science*, *255*, 1391-1397.

Bell, David R., et al. (2003), Hydroxide in olivine: A quantitative determination of the absolute amount and calibration of the IR spectrum, *Journal of Geophysical Research (Solid Earth)*, *108*(B2), ECV 8-1.

Bertelmann, D., et al. (1985), Zum Temperaturverhalten von Sanidinen: Die Ausnahmerolle der Eifel Sanidin-Megakristalle, *Neues Jahrbuch für Mineralogische Abhandlungen*, *152*, 123-141.

Cagniard, L. (1953), Basic Theory of the Magneto-Telluric Method of Geophysical Prospecting, *Geophyics*, *18*(3), 603-635.

Chen, C.-c., and C.-s. Chen (2002), Sanyi-Puli conductivity anomaly in NW Taiwan and its implication for the tectonics of the 1999 Chi-Chi earthquake, *Geophys. Res. Lett.*, *29*(8), 1166.

815 Clayhold, J. A., and M. D. S. B. M. Kerns, D. W. Rench, G. Logvenov, A. T. Bollinger, and I.
816 Bozovic (2008), Combinatorial measurements of Hall effect and resistivity in oxide films, *Rev. Sci.*
817 *Instrum.*, *79*, 033908

818 Conrad, H., and D. Yang (2010), Influence of an applied dc electric field on the plastic deformation
819 kinetics of oxide ceramics, *Philosophical Magazine*, *90*(9), 1141-1157.

820 Constable, S., and A. Duba (1990), Electrical conductivity of olivine, a dunite and the mantle, *J.*
821 *Geophys. Res.*, *95*, 6967-6978.

822 Cygan, R. T., and A. C. Lasaga (1986), Dielectric and polarization behavior of forsterite at elevated
823 temperatures, *Amer. Mineral.*, *71*, 758-766.

824 Dobrovolsky, I. P., et al. (1989), Theory of electrokinetic effects occurring at the final stage in the
825 preparation of a tectonic earthquake, *Pys. Earth Planet. Int.*, *57*, 144-156.

826 Duba, A., and S. Constable (1993), The electrical conductivity of a lherzolite, *J. Geophys. Res.*, *98*,
827 11885-11899.

828 Freund, F., and H. Wengeler (1982), The infrared spectrum of OH--compensated defect sites in C-
829 doped MgO and CaO single crystals, *J. Phys. Chem. Solids*, *43*, 129-145.

830 Freund, F., and M. M. Masuda (1991), Highly mobile oxygen hole-type charge carriers in fused silica,
831 *J. Mater. Res.*, *8*, 1619-1622.

832 Freund, F., et al. (1993), Critical review of electrical conductivity measurements and charge
833 distribution analysis of magnesium oxide, *J. Geophys. Res.*, *98*(B12), 22209-22229.

834 Freund, F., et al. (1994), Positive hole–type charge carriers in oxide materials, in *Grain Boundaries*
835 *and Interfacial Phenomena in Electronic Ceramics*, edited by L. M. Levinson, pp. 263-278, Amer.
836 Ceram. Soc., Cincinnati, OH.

837 Freund, F. T. (2003), On the electrical conductivity structure of the stable continental crust, *J.*
838 *Geodynamics*, *35*, 353-388.

839 Freund, M. M., et al. (1989), Highly mobile oxygen holes in magnesium oxide, *Phys. Rev. Lett.*,
840 *63*(Nov. 6, 1989), 2096-2099.

841 Frost, B. R., et al. (1989), Grain boundary graphite in rocks and impolication for high electric
842 conductivity in the lower crust, *Nature*, *340*, 6229.

843 Frost, B. R., and K. Bucher (1994), Is water responsible for geophysical anomalies in the deep
844 continental crust?, *Tectonophysics*, *231*, 293-309.

845 Fuji-ta, K., et al. (2004), Electrical conductivity measurement of granulite under mid- to lower crustal
846 pressure-temperature conditions, *Geophys. J. Inter.*, *157*, 79-86.

847 Glover, P. W. J., and F. J. Vine (1992), Electrical conductivity of carbon-bearing granulite at raised
848 temperatures and pressures, *Nature*, *360*(24), 723-726.

849 Glover, P. W. J. (1996), Graphite and electrical conductivity in the lower continental crust: A review,
850 *Physics and Chemistry of The Earth*, *21*(4), 279-287.

851 Griscom, D. L. (1990), Electron spin resonance, *Glass. Sci. Technol.*, *4B*, 151-251.

852 Haak, V., and R. Hutton (1986), Electrical resistivity in continental lower crust, in *Nature of Lower*
853 *Continental Crust*, edited by D. A. C. J. B. Dawson, J. Hall, and K. D. Wedepohl, pp. 35-49, Geol.
854 Soc. Spec. Publ., London.

855 Henderson, B., and J. E. Wertz (1977), *Defects in the Alkaline Earth Oxides*, Taylor & Francis,
856 London.

857 Hyndman, R. D. (1988), Dipping seismic reflectors, electrically conductive zones, and trapped water
858 in the crust over a subducting plate, *Journal of Geophysical Research*, *93*(B11), 13391-13405.

859 Hyndman, R. D., et al. (1993), The origin of electrically conductive lower continental crust: saline
860 water or graphite?, *Physics of the Earth and Planetary Interiors*, *81*(1-4), 325-345.

861 Iio, Y., et al. (2002), Water-weakened lower crust and its role in the concentrated deformation in the
862 Japanese Islands *Earth and Planetary Science Letters*, *203*(1), 245-253.

863 Karato, S.-i. (2011), Water distribution across the mantle transition zone and its implications for global
864 material circulation, *Earth and Planetary Science Letters*, *301*(3-4), 413-423.

865 Kathrein, H., and F. Freund (1983), Electrical conductivity of magnesium oxide single crystal below
866 1200 K., *J. Phys. Chem. Solids*, *44*, 177-186.

867 Khan, A., and T. J. Shankland (2011a), A geophysical perspective on mantle water content and
868 melting: Inverting electromagnetic sounding data using laboratory-based electrical conductivity
869 profiles, *Earth and Planetary Science Letters*, *317-318*, 27-43.

870 Khan, A., and T. J. Shankland (2011b), A geophysical perspective on mantle water content and
871 melting: Inverting electromagnetic sounding data using laboratory-based electrical conductivity
872 profiles, *Earth and Planetary Science Letters*, *317*, 27-43.

873 Kittel, C. (1980), *Introduction to Solid State Physics*, J. Wiley & Sons, New York.

874 Kriegler, R. J., and H. L. Welch (1968), Induced infrared fundamental band of hydrogen dissolved in
875 solid argon, *Canad. J. Phys.*, *46*(10), 1181-1189.

876 Lee, C. D., et al. (1983), Electrical conductivity models for the continental crust based on laboratory
877 measurements on high-grade metamorphic rocks, *Geophys. J. Int.*, *72*(2), 353-371.

878 Lempicki, A. (1953), The Electrical Conductivity of MgO Single Crystals at High Temperatures,
879 *Proc. Phys. Soc. B*, *66*(4), 281-.

880 Litovchenko, A. S., and V. V. Mazykin (1984), Dehydroxylation Effect upon Electrical Conduction of
881 Mica, *physica status solidi (a)*, *81*(1), K47-K50.

882 Liu, J.-L., et al. (1999), Studies of electrical properties of rocks under high temperature and pressure,
883 *Acta Seismologica Sinica*, *12*(1), 99-108.

884 Marfunin, A. S. (1979), *Spectroscopy, Luminescence and Radiation Centers in Minerals*, 257-262 pp.,
885 Springer Verlag, New York.

886 Martens, R., et al. (1976a), Hydrogen release during the thermal decomposition of magnesium
887 hydroxide to magnesium oxide, *J. Catalysis*, *44*, 366-372.

888 Martens, R., et al. (1976b), Hydrogen release during the thermal decomposition of magnesium
889 hydroxide to magensium oxide, *J. Catalysis*, *44*, 366-372.

890 Mathez, E. A. (1987), Carbonaceous matter in mantle xenoliths: Composition and relevance to the
891 isotopes, *Geochim. Cosmochim. Acta*, *51*, 2339-2347.

892 Merzer, M., and S. L. Klemperer (1997), Modeling low-frequency magnetic-field precursors to the
893 Loma Prieta earthquake with a precursory increase in fault–zone conductivity, *Pure Appl. Geophys.*,
894 *150*, 217-248.

Meunier, M., et al. (1983), Electrical conduction in biotite micas, *J. Appl. Phys.*, *54*, 896-.

Miller, G. H., et al. (1987), The natural occurrence of hydroxide in olivine, *Phys. Chem. Minerals*, *14*, 461-472.

Mitzutani, H., et al. (1976), Electrokinetic phenomena associated with earthquakes, *Geophys. Res. Lett.*, *3*, 365 - 368.

Nekut, A., et al. (1977), Deep Crustal Electrical Conductivity; Evidence for Water in the Lower Crust, *Geophysical Research Letters*, *4*(6), 238-242.

Nover, G. (2005), Electrical Properties of Crustal and Mantle Rocks – A Review of Laboratory Measurements and their Explanation, *Surveys in Geophysics*, *26*(5), 593-651.

Nover, G., et al. (2005), Promotion of graphite formation by tectonic stress – a laboratory experiment, *Geophysical Journal International*, *160*(3), 1059-1067.

Olhoeft, G. R. (1976), Electrical properties of rocks in *Physics and Chemistry of Rocks and Minerals*, edited by R. J. G. Strens, pp. 261-278, Wiley, London.

Olhoeft, G. R. (1981), Electrical properties of granite with implications for the lower crust, *J. Geophys, Res.*, *86*(B2), 931-936.

Pacchioni, G., et al. (1993), Measures of ionicity of alkaline-earth oxides from the analysis of ab initio cluster wave functions, *Phys. Rev. B*, *48*, 11573–11582.

Parkhomenko, E. I. (1967), *Electrical Properties of Rocks*, 314 pp., Plenum Press, New York, NY.

Parkhomenko, E. I. (1982), Electrical Resistivity of Minerals and Rocks at High Temperature and Pressure, *Rev. Geophys. Space Phys.*, *20*, 193.

Patro, B. P. K., et al. (2005), Electrical structure of the crust below the Deccan Flood Basalts (India), inferred from magnetotelluric soundings, *Geophys. J. Int.*, *163*, 931-943.

Qin, X., et al. (1992), Conductivity structure of crust in the Tangshan seismic area and the possibility of exploring potential seismic sources by magnetotelluric method, *Acta Seismologica Sinica*, *5*(2), 355-365.

Roberts, J. J., et al. (1999), Carbon-enhanced electrical conductivity during fracture of rocks, *J. Geophys. Res.*, *104*(B1), 737-747.

Rossman, G. R. (1996), Studies of OH in nominally anhydrous minerals, *Phys. Chem. Minerals*, *23*, 299-304.

Sempolinski, D. R., and W. D. Kingery (1980), Ionic conductivity and magnesium vacancy mobility in magnesium oxide, *J. Amer. Ceram. Soc.*, *63*, 664-669.

Shankland, T. J., et al. (1997), Increase in electrical conductivity with pressure as an indicator of conduction through a solid phase in midcrustal rocks, *J. Geophys. Res.*, *102*(B7), 14,741-714,750.

Speit, R., and G. :ehmann (1982), Radiation defects in feldspars, *Physics and Chemistry of Minerals*, *8*, 77-82.

Takahashi, I., et al. (2007), Anomalous geoelectrical and geomagnetic signals observed at Southern Boso Peninsula, Japan, *Annals of Geophysics*, *50*(1), 123-135.

Teisseyre, R. (1983), Premonitory mechanism and resistivity variations related to earthquake *Pure and Applied Geophysics 121*(2), 297-315.

934 Unsworth, M., et al. (1999), High-resolution electromagnetic imaging of the San Andreas fualt in
935 Central California, *J. Geophys. Res.*, *104*(B1), 1131-1150.

936 Vanyan, L. L., and A. O. Gliko (1999), Seismic and electromagnetic evidence of dehydration as a free
937 water source in the reactivated crust, *Geophysical Journal International*, *137*(1), 159-162.

938 Wang, D., et al. (2012), Electrical conductivity of amphibole-bearing rocks: influence of dehydration,
939 *Contributions to Mineralogy and Petrology 2012*(7 February 2012), 1-9.

940 Wannamaker, P. E. (1994), Fluids in the Earth's crust: Electromagnetic constraints on existence and
941 distribution, *U.S. Geol. Surv. Open file Rep.*, *94-228*, 162-177.

942 Wannamaker, P. E. (1999), Comment on "The petrologic case for a dry lower crust" by Yardley,
943 B.W.D. and J.W. Valley, *J. Geophys. Res.*, *subm.*

944 Wanvik, J. E. (2000), Norwegian anorthosites and their industrial uses, with emphasis on the massifs
945 of the Inner Sogn-Voss area in western Norway, *Norges geologiske undersøkelse Bulletin*, *436*, 103-
946 112.

947 Wuensch, B. J., et al. (1973), Cation self-diffusion in single crystal MgO., *J. Chem. Phys.*, *58*(12),
948 5258-5266.

949 Wuensch, B. J., et al. (1991), The mechanisms for self-diffusion in magnesium oxide., in *Point Defects*
950 *and Related Properties of Ceramics.*, edited by T. O. Mason and J. L. Roubort, pp. 79-89.

951 Yang, X. (2011), Orientation-related electrical conductivity of hydrous olivine, clinopyroxene and
952 plagioclase and implications for the structure of the lower continental crust and uppermost mantle
953 *Earth and Planetary Science Letters*, *317-318*, 241-250.

954 Yardley, B. W. D., and J. W. Valley (1997), The petrologic case for a dry lower crust, *J. Geophys.*
955 *Res.*, *102*(B6), 12,173-112,185.

956 Yardley, B. W. D., et al. (2000), Origin of retrograde fluids in metamorphic rocks *Journal of*
957 *Geochemical Exploration*, *69-70*, 281-285.

958 Yardley, B. W. D., and J. W. Valley (2000), "The petrologic case for a dry lower crust" Reply to a
959 comment by P.E. Wannamaker, *J. Geophys. Res.*, *105*(83), 6057-6068.

960 Yoshida, S., et al. (1998), Electrical potential changes prior to shear fracture in dry and saturated
961 rocks, *Geophys. Res. Lett.*, *25*(10), 1577-1580.

962 Yoshino, T., and F. Noritake (2011), Unstable graphite films on grain boundaries in crustal rocks,
963 *Earth and Planetary Science Letters*, *306*(3-4), 1826-1192.

964 Young, K. F., and H. P. Frederikse (1973), Compilation of the static dielectric constants of inorganic
965 solids, *J. Phys. Chem. Reference Data*, *2*, 313-409.

966